Stony Brook University

Thermal Spray Process Variability and Methods of Control

A Thesis Presented

by

Travis Wentz

to

The Graduate School

in Partial Fulfillment of the

Requirements

for the Degree of

Master of Science

in

Mechanical Engineering

Stony Brook University

August 2009

Stony Brook University

The Graduate School

Travis Wentz

We, the thesis committee for the above candidate for the

Master of Science degree, hereby recommend

acceptance of this thesis.

Sanjay Sampath – Thesis Advisor

Director of CTSR, Professor, Department of Material Science

Toshio Nakamura – Chairperson of Defense

Professor, Department of Mechanical Engineering

Chad Korach – Assistant Professor, Depart of Mechanical Engineering

This thesis is accepted by the Graduate School

Lawrence Martin
Dean of the Graduate School

Abstract of the Thesis

Thermal Spray Process Variability and Methods of Control

by

Travis Wentz

Master of Science

in

Mechanical Engineering

Stony Brook University

2009

The controllability of the thermal spray process is an interesting topic that has recently gained attention. The thermal spray process itself is stochastic in nature. A thermal sprayed coating is comprised of a great amount of small particles that are subjected to a violent high energy environment, melted and then solidified all within a fraction of a millisecond. What is the extent to which the outcome of this turbulent process can be predicted? Can coating properties be predicted with 100% confidence? Unfortunately, at this point in time the answer is no. So, what can be done to achieve a high level of confidence?

A series of experiments were conducted at the Center for Thermal Spray Research at Stony Brook University to measure and analyze the variability and controllability of several aspects of the thermal spray process. This included the in-flight particle state measured by two optical sensors, Accuraspray and DPV2000, along with the mechanical and physical properties of the finished coating. In this investigation, the spray material used was Yttria Stabilized Zirconia (YSZ). Two powder morphologies were studied; Hollow Spherical (HOSP) and Fused and Crushed (FC). The focus on this material was due to its application as a thermal barrier coating and the market need in the gas turbine industries.

First-order process maps were generated and utilized to visualize the correlation between spray torch input parameters and the particle's in-flight characteristics (i.e.

temperature and velocity, melting index and kinetic energy). The sets of input conditions were generated per "Design of Experiments" methods to single out the effects of individual parameter; argon flow rate, hydrogen flow rate, and current.

The variability of each process map condition was investigated by making a series of five first-order process maps and five coatings using the Accuraspray, DPV2000, and In-Situ Coating Property (ICP) sensors. Accuraspray and DPV2000 were used to measure in-flight particle characteristics, i.e. temperature and velocity. The ICP sensor, developed at the Center for Thermal Spray Research, was used to measure the curvature and the temperature of the substrate during the coating's deposition and during cooling. These experiments provided the unique variability inherent to each spray condition.

Production environments were also accounted for where YSZ is used to coat specific hot section gas turbine engine parts. The Accuraspray diagnostic system and the ICP sensor were used to measure in-flight particle characteristics and to analyze coating deposition. An injection optimization experiment was performed and found to have significant effects on process map repeatability, deposition efficiency, and coating properties.

The proposed control methods go beyond reading process maps to plan an experiment. Process map data was used to develop a control algorithm that automatically calculates torch input parameters. This algorithm was used to achieve a desired point on the material-torch specific TV space. Also, the algorithm was used to fine tune the torch parameters and repeat a desired particle state within a small range of temperature and velocity, ±15°C and ±2m/s. Coatings were made using this tuning procedure and compared to coatings made while using fixed torch settings.

Table of Contents

List of Figures

List of Tables

List of Acronyms

CTSR:	Center for Thermal Spray Research
TBC:	Thermal Barrier Coating
YSZ:	Yttria Stabilized Zirconia
HOSP:	Hollow Spherical
FC:	Fused and Crushed
ICP:	In-Situ Coating Property
CCD:	Charge Coupled Device
LED:	Light Emitting Diode
DoE:	Design of Experiment
TV or T&V:	Temperature and Velocity
MI:	Melting Index
KE:	Kinetic Energy

Acknowledgments

This research project would not have been possible without the help and support of many people over the years. I would like to take this opportunity to express my gratitude to my advisor Professor Sanjay Sampath who has given me invaluable support and guidance throughout my academic career. He has always been very encouraging and a great mentor that I am honored to have studied under. The lessons and skills learned from Professor Sampath will be regarded as priceless assets in the years to come.

I am grateful to all of my fellow CTSR students that I have worked with. I would like to thank Jose Colmenares-Angulo and Antonio Caccavale for the countless number of hours that we spent together designing experiments, spraying samples, and analyzing data. I would like to thank the CTSR alumni, Alfredo Valarezo, Brian Choi, Yang Tan, Vasudevan Srinivasan, Anirudha Vaidya, and Wei-Guang Chi for passing on their invaluable knowledge and the techniques that they have developed through many years of experience. Many thanks also to the faculty and students that attended CTSR's weekly group meetings and provided suggestions and feedback. I believe these meetings were very beneficial for preparing for my thesis defense and will be reflected upon when future projects arise. I have always appreciated that CTSR is a large, diverse group comprised of intelligent people from around the world. I appreciate that I had the opportunity to learn a lot about other cultures while working together in a friendly productive environment.

I would like to express my gratitude towards the United States Air Force, who has supported this research through grant number FA8650-07-C-2732, monitored by Ruth Sikorski. Their invaluable contribution has been of great benefit to myself and to CTSR, allowing us to expand our knowledge of TBCs and the thermal spray process and provide useful information to the thermal spray community. I would also like to convey thanks to Manmohan Tuli, Tinker Air Force Base, for the opportunity to experiment in a production environment. The exposure to this environment was privileged experience that I am grateful for.

Last but not least, to the faculty and staff of the mechanical engineering department I am grateful for all of the teachings and guidance provided to me throughout my graduate and undergraduate career at Stony Brook University. I was always motivated by their enthusiasm for engineering and teaching as well as their expansive knowledge. It was always a pleasure to attend their lectures and partake in laboratory experiments.

1. Introduction

In today's economy there is an ongoing struggle to increase the efficiency of energy production. The term 'energy production' is not limited to only the well known power stations that generate electricity for our cities and communities, but extends to propulsion for jet aircraft and other modes of transportation that are a critical to the nations infrastructure and its military defense. Commercial flight is an enormous industry that spans the globe, connecting parts of the world that were previously inaccessible and isolated. According to the National Air Traffic Controllers Association (NATCA), as of June 21 of 2009 there are around 29,000 commercial flights in U.S. skies within any given day. The propulsion mechanism common to a majority of these aircraft is the jet engine. The jet engine gives these aircraft such extraordinary capabilities. They are able to endure long range flights for extended periods of time without refueling. They are able to carry incredible loads and fly at higher altitudes than ever before.

The jet engine has always been a focal point for the commercial flight industry in a business sense because it is so closely linked to cost. How efficiently the engine can use its fuel to produce thrust directly affects the cost of the flight and the amount of fuel used. On top of the fuel cost, when it undergoes combustion it releases a number of byproducts that are detrimental to the environment, the most influential being Carbon Dioxide. The CO_2 emissions from commercial flights are one of the leading contributors to the present global warming crisis. According to the Google maps flight emission calculator, a flight from New York's JFK airport to Narita, Tokyo (6,737 miles) would release approximately 2,630 lbs of CO_2 per passenger. In comparison, a flight from New York to Los Angeles (2,472 miles) would produce 965 lbs per passenger of CO_2 emissions. Efficient engines are the key to cleaner healthier future.

Jet propulsion engines are also used within the military sector on a number of different aircraft, the most well known being the fighter jet. The demands on fighter jet engines are much higher than those for commercial aircraft primarily due to the nature of the aircraft and its mission. For instance, the fighter aircraft must be light and

maneuverable to avoid enemy fire. This restricts the amount of fuel that can be carried as a heavier plane is slower to react, becoming an easy target. With a small amount of fuel available the aircraft has a limited operating range. Limited range means that the aircraft would need to be launched closer to the enemy to reach the target, which puts many people in a potentially dangerous situation. To extend the operating range of the aircraft, the engine efficiency must be raised. Because of the demands of combat, the fighter aircraft's engines undergo a higher number of loading and unloading cycles as the pilot is trying to outmaneuver the enemy. These varying demands for thrust lead to more engine stresses due to transient operation. As a precaution, these engines are routinely inspected and rebuilt to combat these harsh operating conditions and avoid a catastrophic failure.

Land based turbine engines are used primarily for electricity production. These engines can be used to provide power to anything from a city to a small college campus. The demand on these engines is low because they are typically run at a steady state operating condition for long periods of time. Since the energy is produced at a constant rate, and the demand for electricity will vary throughout the day, power production is usually regulated by storing excess electricity in some form of potential energy (i.e. battery, water tower, etc.).

Besides fuel cost, another concern common to all gas turbine engines is operating temperature. The upper limit of operating temperature is governed primarily by the material properties of the metals used within the engine. High operating temperatures cause the metals to become weak and loose their structural integrity, causing a catastrophic failure. On the ground this means shutting down the power station until the parts can be repaired. On the other hand, if the failure occurs in an aircraft engine the results could be deadly. Why is there so much attention focused on the operating temperature? Based on thermodynamic law, the engine's operating temperature is a main contributor to efficiency. An increase in operating temperature directly results in an increase in efficiency, leading to reduced fuel consumption and money saved. What solutions are available that will lead to a more efficient gas turbine engine without sacrificing the internal components?

1.1 Thermal Barrier Coatings (TBCs)

1.1.1 What is a TBC?

Thermal barrier coatings are materials with a very low thermal conductivity. A high melting point is an important quality for a TBC to have so that it can be exposed to a hot environment without a loss of integrity. In the realm of gas turbine engines, TBCs can be applied to land based power producing turbines and aero engines used for jet propulsion. The purpose is to insulate and protect underlying super-alloys from exposure to the high temperatures (~1300 K) and hazardous erosive environment created by these engines. Figure 1.1-1 displays the application of a TBC to a blade from a gas turbine engine. The TBC is typically deposited on top of a bond coat for a number of reasons. It can reduce the amount of residual stress that is felt by the coating and the substrate and helps to prevent delamination. It also can absorb some of the stresses that occur as a result of the substrate deforming. The application of TBCs to gas turbine engines leads to a raising combustion temperature, making them more efficient, thus saving more fuel.

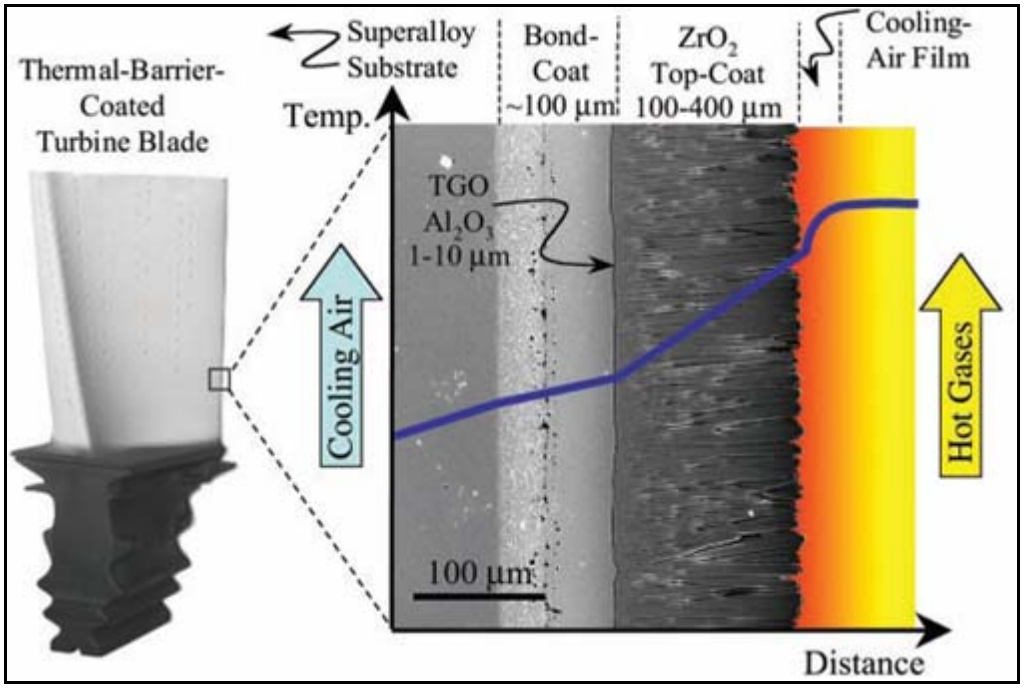

Figure 1.1-1. Diagram of a TBC applied to a turbine blade [1].

While some engineers utilize the benefits of a TBC in their design process, some TBCs are not considered to be 'prime reliant.' This means that the engine is designed to operate without the coating in place and added later only for extra protection of engine components. Much research is underway to make the coatings more predictable and reliable so that engine function will depend on them. One problem under investigation is the repeatability of a coating and the coating process. There is a desire to control the process to the extent that each coating produced has the same properties. The life of the coating is then predicted with low variability and high confidence.

The life cycle of current coatings is somewhat unpredictable. Coatings are unexpectedly failing in both infant and mature stages, which may cause a catastrophic failure in the next generation engines that might be designed to rely on TBCs for thermal protection. Some of these failures can be contributed to a thermally grown oxide that occurs naturally between the substrate and TBC, causing delamination.

1.1.2 TBC's Thermal-Mechanical Properties

As a result of thermal spraying a TBC, some unique characteristice are created that differ from the bulk material. Studies show that there is a relationship between the density/porosity of a thermal sprayed coating with its thermal conductivity [2-6]. Typically, when a coating is sprayed so that there are many cracks, pores, and splat interfaces, the resulting thermal conductivity is significantly lower than the bulk value. The defected microstructure of the TBC also causes the coating to have a non-linear elastic modulus. This phenomenon was studied and modeled by Nakamura and Liu in [7]. When the substrate is under strain the motion between splats and the opening of cracks relieves some coating stresses and decreases its elastic modulus. This is also found in high temperature application where thermal expansion of the coating and substrate cause stresses to develop due to the different expansion rates.

The deposition of thermal sprayed TBCs also leads to residual stresses due to three major factors; peening, quenching, and thermal mismatch. The peening stresses are

caused by the transfer of kinetic energy from the particles to the substrate and subsequent layers of the coating. The quenching stress is caused by the solidifying particle's reduction in volume sue to a large reduction in its temperature. Finally, the thermal mismatch stress is created because of the difference in thermal expansion coefficients. From the time the spraying ends until both coating and substrate come to an equilibrium temperature the coating and substrate are shrinking at different rates.

1.1.3 Purpose for TBCs in Gas Turbine Engines

Thermal barriers are thought of as insulators that reduce the amount of heat flow from one body to another, whether it is any combination of solid-liquid-gas bodies. As many engineers are concerned with reducing the amount of heat loss, or energy wasted, from a power producing system, these coatings are of great interest. This study was motivated by the aerospace and power generation industries because a great number of gas turbine engines are currently using TBCs as a means of protecting parts within their hot sections that reach temperatures around 1600 K. These parts include the combustion chambers, exhaust turbines, and exhaust nozzle (see Figure 1.1-2).

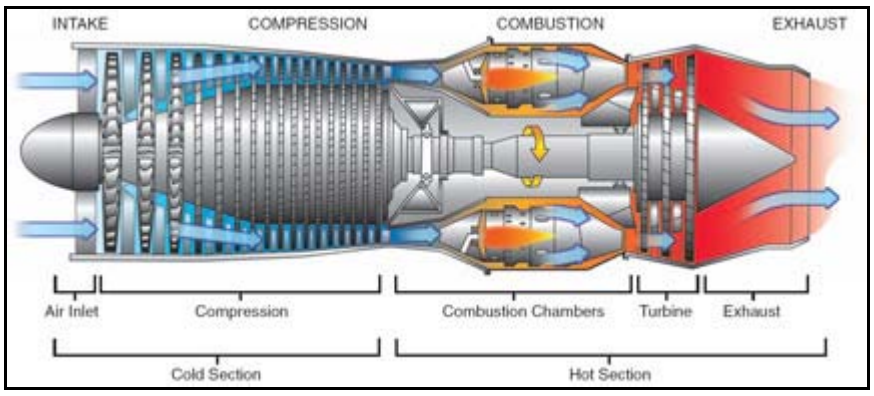

Figure 1.1-2. Diagram of a gas turbine engine used for propulsion [8].

The thermodynamic cycle of a gas turbine engine is called the Brayton cycle, shown in Figure 1.1-3. For a simplified analysis, it is assumed that the working fluid

(air) undergoes isentropic compression, isobaric heating, isentropic expansion, and an isobaric heat rejection to the environment.

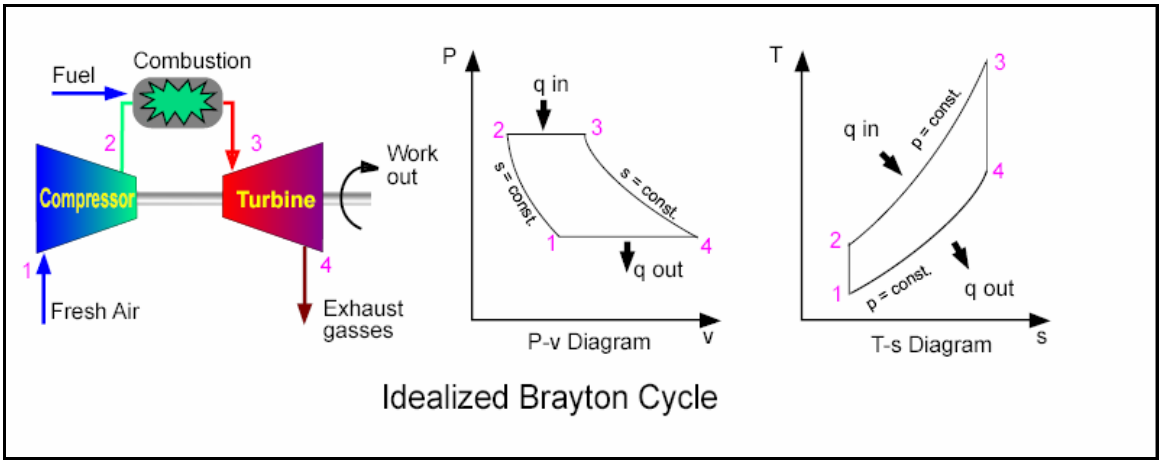

Figure 1.1-3. Diagram of ideal Brayton cycle. Air enters the compressor (1) at ambient conditions undergoes isentropic compression. The high pressure air (2) is heated by an isobaric combustion process and then sent to an expansion turbine (3) where it undergoes an isentropic expansion. This creates power to drive the compressor. Finally the air is exhausted from the engine (4). Image taken from http://en.wikipedia.org/wiki/Brayton_cycle, June 2009.

The energy balance equation for the Brayton cycle is shown below in equation 1.

$$W = Q_{in} - Q_{out} \qquad \textbf{1}$$

W: work output of the cycle; work of turbine - work of compressor
Q_{in}: heat added to the system by combustion
Q_{out}: heat rejected as exhaust

The efficiency of the Brayton cycle is described below by equation 2.

$$\eta = \frac{W}{Q_{in}} = \frac{Q_{in} - Q_{out}}{Q_{in}} = 1 - \frac{Q_{out}}{Q_{in}} = 1 - \frac{mC_p(T_1 - T_4)}{mC_p(T_3 - T_2)} = 1 - \frac{\Delta T_{out}}{\Delta T_{in}} \qquad \textbf{2}$$

η: efficiency
m: mass of working fluid
C_p: specific heat of air
$T_{1\text{-}4}$: temperatures at points in the cycle
ΔT_{out}: temperature drop at exhaust
ΔT_{in}: temperature change at combustion

Equation 2 simply states that the efficiency of the Brayton cycle is equal to the amount of work output divided by the difference of heat added and heat lost. This is also directly related to the temperature differences of the combustion and exhaust processes. In order

to increase the efficiency of the Brayton cycle the amount of heat input must increase and the amount of heat rejection must decrease.

Since it is not practical to reduce the inlet temperature, the engine must burn hotter to achieve this goal. This causes a problem for the current superalloys that are used in today's aero engines. The burn rate is controlled to keep the engine operating within a safe range of temperature that does not damage engine parts. But what if we had better materials or a way of insulating the super alloys from the intense heat? While the superalloy engine materials are already very expensive, coatings offer a much less expensive solution. This is where the TBC comes into play. It acts as a heat shield and keeps the super alloy temperature relatively cool, considering its safe operating limit, while raising the engine operating temperature [9].

The problem with present TBCs is that they are not 100% reliable. They are not expected to last long enough to provide the necessary sustained heat barrier. There are currently deep investigations being performed in order to understand the failure methods of TBCs in aero engines in order to solve this problem [9]. So why are they used today? They do provide some heat protection to the super alloy and help it resist many problems related to high temperature operation. Occasional failures of coatings are not critical to the engines operation and are detected during routine inspections.

1.1.4 Yttria Stabilized Zirconia as a TBC

TBCs can be created using many different materials. A very common and widely used material is Yttria Stabilized Zirconia. Although any material with a low thermal conductivity can be used as a TBC, YSZ's thermal conductivity is much lower than other ceramics at elevated temperatures (~2.3 W/m·K at 1000°C) [1]. YSZ also has a high melting point of ~2700 C [10]. There are also other characteristics to consider than only thermal conductivity and a high melting point [10]. Some materials will undergo a phase transformation when brought to a high temperature. The phase transformation causes a significant volume change making the material difficult to work with. This is typically undesirable for a TBC coating. Pure Zirconia demonstrates this phase change and is the

reason why its crystal structure must be stabilized by adding a small percentage of Yttria. YSZ also has a relatively low density (~4.8 g/cc) that is greatly considered when a coating is applied to moving parts such as turbine blades. When thermal sprayed, YSZ has a relatively low elastic modulus (~50 GPa) that plays an important role in coating toughness. This low modulus allows the coating to be resilient and enables it to undergo some deformation without brittle fracture. This property is essential when some residual stresses from the deposition process exist, when stresses arise due to thermal mismatch between the coating and substrate, and when outside forces are present causing the coating-substrate pair to deform.

1.1.5 Creating a TBC Coating

There are many processes that can be used to deposit a TBC. The thermal spraying process is one that creates a unique microstructure, decreasing the already low thermal conductivity of YSZ by introducing a large amount of defects into the microstructure. Thermal spray is widely used today and has a broad range of applications [11]. Parts can be sprayed with wear resistant coatings that protect underlying materials and extend the life of the part. Worn parts are repaired by adding a layer of thermal sprayed material onto it, building it up larger than the final shape, and then machining the part back into tolerance. One field of thermal spray involves the application of coatings that are used as sensors such as thermocouples and strain gages. The mobility of the thermal spray is an important aspect of the process. One advantage over other coating methods is that a thermal spray coating can be applied to parts or a structure in the field without requiring a large amount of heavy equipment. Also, the structure does not need to be disassembled and can be sprayed as is. This is especially advantageous for large jobs, such as bridges, or where parts not able to be removed.

The process of thermal spraying involves transferring energy to small particles, in order to melt them, and projecting them toward a substrate (Figure 1.1-4). The substrate can be anything from a small sample of aluminum used for laboratory experiment to a combustor can in a gas turbine engine that will be used in an aircraft. The particles impact the substrate and then rapidly solidify, causing layers upon layers of “splats” to be deposited. These “splats” are the building blocks of all thermal spray coatings. The

relative motion shown in the figure is how the torch is moving along with respect to the substrate. The path of motion is based upon the size of the spray plume and the size of the part. Relative velocity must be carefully chosen as it directly affects the coating properties.

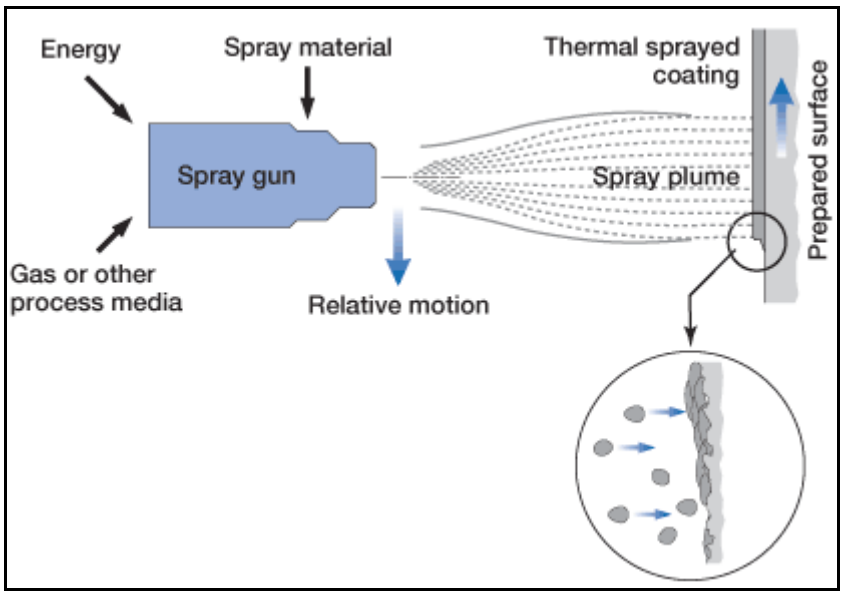

Figure 1.1-4. Diagram of the thermal spray coating process showing the spray gun, spray plume of plasma gas and spray material, substrate, and splat buildup (clockwise from top left) [12].

At SUNY Stony Brook's Center for Thermal Spray Research, a Sulzer Metco 7mb Ar-H_2 plasma torch was used to create the YSZ coatings in the following experiments. The plasma torch is a popular technique because it provides the adequate thermal energy needed to melt the ceramic powder. Typically the particle size of the powder ranges from 10µm to 150µm, which leads to a wide variety of melting state where the particle can be un-melted, semi-melted, or fully melted. The variety of melting states is one contributor to the unique microstructure of thermal sprayed YSZ. Also, attention must be paid to the choice of powder morphology which is another main contributor to the coating's microstructure. The two morphologies used in this study were hollow spherical (HOSP) and fused and crushed (FC), shown in Figure 1.1-5. The powder is usually deposited at a rate from 10 to 50 microns per pass while a robot is moving the plasma torch in a prescribed 'ladder' pattern. The use of the robot ensures consistency in traverse speed as well as spray distance.

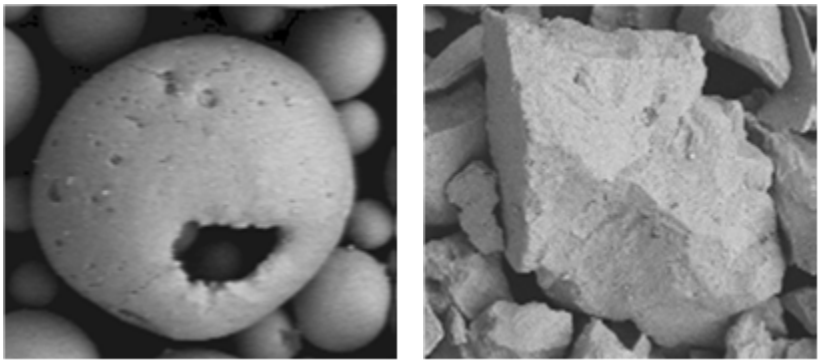

Figure 1.1-5. Micrograms of hollow spherical (left) and fused & crushed (right) Yttria stabilized Zirconia powder morphologies [13].

1.2 Reliability-Repeatability-Reproducibility

What good is any engineering problem that can not be solved consistently? The thermal spray process, by nature, is a stochastic process. There are many variables that can influence coating properties. These include, but are not limited to, plasma gas choice, flow rates of plasma gases, size of nozzle, type of injection, feed rate of powder, feedstock powder particle size distribution, morphology of powder, etc. Also, the path of individual particles entering the plasma stream cannot be accurately represented. This is due in part to the turbulent gas flow exiting the spray torch and each unique particle interacting with it in a different way. The injected particles are not uniform in size, shape or mass, thus each particle will have its own unique interaction with the plasma gas jet.

This plethora of variables has driven scientists to develop spray equipment that is highly controllable. For example, a contemporary plasma torch controller can set, measure, and adjust the flow rates of the plasma gasses to within a tenth of one standard liter per minute. The power input to the torch can also be controlled by different methods. The torch operator can fix the current input within one amp or the power input to within one kilowatt. The rate of powder injection can also be controlled to a finite level. The rotation of the powder feeding disk can be set with one rpm resolution. Knowing the dimensions of the powder feeding disk groove containing the powder, the precise volumetric amount of feed stock material going to the torch can be calculated and

controlled. This powder feeding is more robust at higher feed rates, where at low feed rates the powder can become clumped together resulting in pulsed feeding.

Another milestone advancing the controllability of the thermal spray process was the integration of robots into the spray booth. Robots are able to consistently follow a spray pattern with a fixed traversing velocity and fixed incident angle. This is highly beneficial to the effort of making coatings with consistent properties because the rate of deposition and the particle impact angle are known to highly influence the coating microstructure.

A monumental breakthrough in thermal spray reliability was the development and incorporation of in-flight particle sensors. These sensors measure properties such as temperature, velocity, and particle diameter while the particles are in flight between the nozzle of the plasma torch and impacting the substrate, sometimes while immersed in the hot plasma gas depending on the measurement location. These sensors gave new insight into what was happening during the coating's creation and led scientists to question if they could link these in-flight particle properties to coating properties. The answer was yes. Strong correlations between in-flight particle states and coating properties were developed. These correlations are being used as a kind of 'road map' to develop coatings with a set of desired properties.

With the capability of measuring in-flight particle characteristics, the interpretation method of the sensor data became the topic of interest. The most common particle characteristics measured by these sensors are temperature and velocity. Some measurements are taken at the individual particle level, resulting in thousands of data points recorded every second. Other measurements are taken as an ensemble, grouping the whole spray stream into a single data point. The question that is repeatedly raised is that if these superficial properties sufficiently describe the particle state or if new grouped parameters are required that incorporate the spray particles physical and thermal properties. In any regard, the measurements of in-flight properties of thermally sprayed particles must be looked at from a statistical point of view. A thermal sprayed coating is made up from many upon many small particles, all with unique in-flight histories. The statistical analyses presented in this paper investigate distributions of particle states and particle state variability associated with specific combinations of spray parameters.

1.3 Thermal Spray Sensors

There are many sensors available today that are used by the thermal spray industry for spray stream monitoring. This study includes the use of the Accuraspray g-3 and the DPV-2000 sensors. Both were used in this study to capture the in-flight temperature and velocity (T and V) of the powder feedstock after it was injected into the plasma plume. The Accuraspray sensor uses an ensemble measuring algorithm while DPV2000 measures individual particles. Both systems have their own set of advantages and disadvantages [14]. Ensemble sensors are able to measure large amounts of particle flow but cannot say anything about individual particle characteristics. On the other hand, single particle sensors can be overwhelmed by a large number of particles but when used properly can show details about the single particles in the spray plume [15]. A detailed description of the theory of measurement and the operation of these sensors can be seen in [16-18].

Measurements in the following experiments were taken at a spray distance where the particles would impact the substrate and accumulate to form the coating. T and V are two measurable parameters that directly influence the coating's microstructure and thermal-mechanical properties. There are of course many others (i.e. grouped parameters melting index and kinetic energy, rate of deposition, particle size, robot speed, spray angle, substrate temperature etc.), some of which are determined from the detailed measurements of individual particle sensors.

Figure 1.3-1 shows the components of the Accuraspray sensor head along with the analog signal sent from the detectors. Twin wavelength pyrometery and time of flight are used by both Accuraspray and DPV2000 to measure temperature and velocity respectively. The pyrometer measures the intensity of thermal radiation and based on the Stefan–Boltzmann equation calculates particle temperature. The velocity is measured using the time shift of the two filtered wavelengths (Figure 1.3-1). The light is first channeled through two optical fibers (point 1) of known spacing. The intensity is then

measured by two detectors (point 3 and 4). The two raw signals (point 5) are compared to find the time separation between corresponding peaks. The known distance between the optical fibers is divided by the time to calculate the velocity. Other information, such as plume position, plume width, and intensity profile were determined using algorithms and data collected from the CCD camera (point 6).

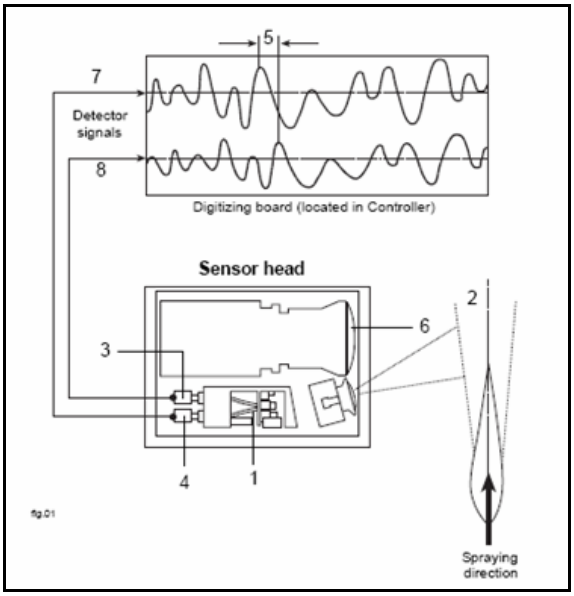

Figure 1.3-1. Accuraspray sensor head showing detector signals. Dual fibers (1) direct light from two different points in the spray stream (2) to detectors (3) and (4). The signals (7 & 8) are sent to the digitizing board. The amount of time (5) for a particle to cross both optical fibers can be precisely calculated. Spray plume geometry and intensity are measured by CCD camera (6) [18].

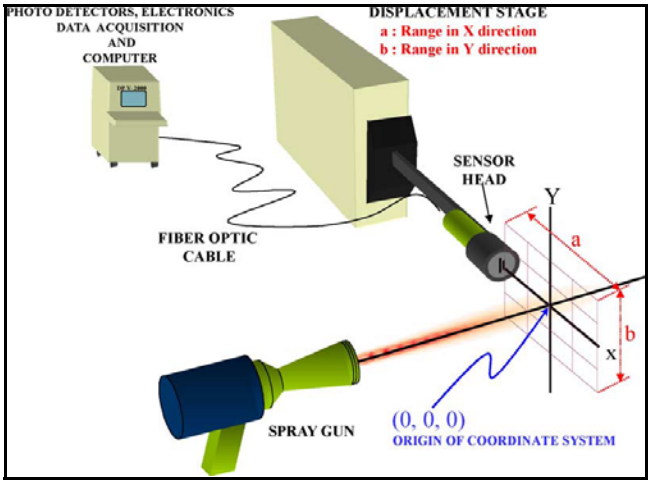

Figure 1.3-2. Schematic of the 'DPV 2000' diagnostic equipment [19]

The DPV2000 will first the move its sensor head to the location of maximum particle flux. The sensor will measure the T and V with the same principle of time of flight and twin wavelength pyrometry, based on thermal emissions [19]. Velocity is calculated using equation 3 and Figure 1.3-3 provided by Technar.

$$V = \frac{TOF}{s} xOpticalMag \qquad \mathbf{3}$$

V:	Particle velocity
TOF:	Time of flight of the particle
s:	Distance between slits
$OpticalMag$:	Constant based on sensor head

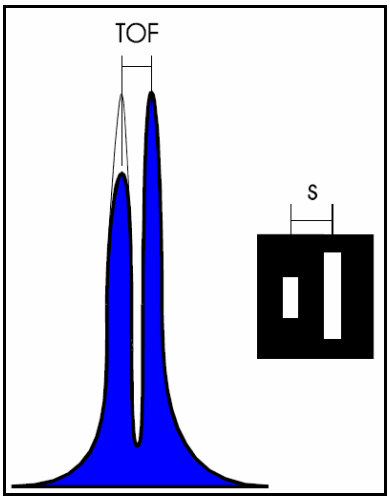

Figure 1.3-3. DPV 2000 principle for velocity measurement [17].

In addition to the in-flight particle sensors, the In-Situ Coating Property (ICP) sensor (developed at the Center for Thermal Spray Research CTSR, Stony Brook) was used to continuously monitor coating deposition during the spraying process. The ICP sensor is unique in that it monitors in real time, giving the operator insight into the evolving coating's characteristics. It measures the substrate's temperature and deflection by means of contact thermocouples and a linear displacement laser. Figure 1.3-4 below shows a photo taken of the ICP sensor in the spray booth before an experiment. The sensor was aligned so that the path of the spray torch is parallel to the substrate's surface, resulting in a fixed spray distance and impact angle. The figure also shows the

arrangement of the distance measuring laser (position 1) and the two contact thermocouples (positions 2 and 3) inside the ICP sensor. The geometry of the substrate and the location of the laser enabled calculation of substrate curvature. The two thermocouples continuously monitor the substrate temperature. These characteristics combined were used for calculations of stress and elastic modulus.

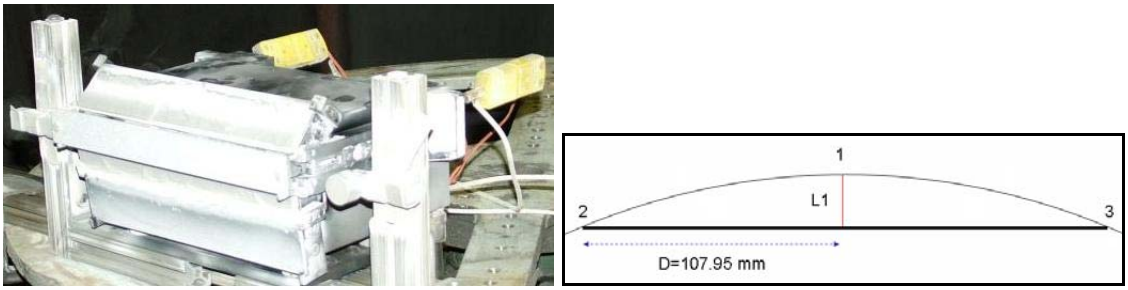

Figure 1.3-4. In-Situ Coating Property sensor (left). Layout (right) showing the position of the linear displacement laser (1) and the two contact thermocouples (2 and 3). Substrate simply supported at both ends (2 and 3).

1.4 Problem Statement

The high demand for energy focuses a lot of attention on efficient methods of its production. Just a one percent increase in efficiency would relate to billions of dollars in fuel savings. For a combustion cycle, the efficiency of the engine is directly related to the combustion temperature. The problem is that there is an upper limit of the combustion temperature that depends on the materials used in the engine. TBCs are one solution to this problem, but they are not yet at the level of reliability where they can be part of the engine design process.

There are many factors that contribute to coating properties and characteristics, details shown in [3, 4, 20-25]. These include powder feedstock, plasma gas flows, powder feed rate, injection gas flow, voltage fluctuations, substrate temperature, substrate thickness, etc. Most thermal spray experiments are designed to study the effects of spray parameters on a coating property, i.e. porosity, thermal conductivity, residual stresses, etc.

The problem addressed in this study is the difficulty to reproduce the exact same coating properties no matter how precise the torch parameters, injection, and substrate characteristics are controlled. The measured in-flight particle state varies from one run to another. Standard industry practice to repeat a coating is to set all controllable parameters to the same as the previous run. This has been proven to result in a varying range of coating properties [13].

In order to reduce variation of coating properties, what aspect of the thermal spray process must be brought to a higher level of control? In most configurations the torch controller is monitoring the flow of gasses and the power input and fixing them to a relatively stable value. Do the small fluctuations lead to significant coating property variability? Will there be any benefits by incorporating particle sensors and diagnostic tools to form a feedback loop tied to the torch controls? Perhaps by taking measurements of in-flight particle characteristics and by measuring deposition characteristics during the process, the coating properties can be predicted in advance. The problem here is to find a formula that will make the connection between the measurements and the finished product. A dynamic technique must be developed that will enable the thermal spray engineer to sufficiently predict the coatings characteristics with a high level of confidence.

1.5 Research Objective

The objectives of this experiment are as follows:

- Conduct background study of TBCs and determine their usage in current technology.
- Research how TBCs are manufactured and what materials are used.
- Understand the benefits that TBCs provide to the gas turbine industry and how they affect the thermodynamic cycle.
- Relate increased efficiency of gas turbine engines to a dollar amount.
- Understand the purpose of process maps and utilize them to analyze data collected from thermal spray experiments.

- Repeat process maps to determine each condition's variability.
- Convert sensor data to properties that better describe individual particle characteristics; melting index and kinetic energy.
- Determine the variability of coating properties when fixing torch parameters and spraying conditions. Properties include thickness, weight, density, residual stress, and elastic modulus.
- Develop and utilize an effective method of trimming large amounts sensor data.
- Study how changing the torch cathode affects TV repeatability.
- Carryout CTSR lab practices in a production environment and compare to standard practice.
- Develop a tuning algorithm that will output a set of torch parameters for a desired particle state. This includes average TV, average MI-KE, TV distributions, and MI-KE distributions.
- Use tuning algorithm to replicate the particle state within a small tolerance and produce coatings. Analyze coating properties and measure variability.
- Make conclusions based on this study about the present state of thermal spray variability and offer solutions for its reduction.

2 Experimental Procedures

The following procedures are part of CTSR's routine for thermal spray experiments. They are always employed in order to keep a stable and controlled process that eliminates any unwanted interference from outside influences. These procedures include:

- Cleaning and preparing consistent substrates to eliminate contamination and attain comparable surfaces on which to deposit the coating.
- Aligning sensors to reduce the error in measurement.
- Optimizing injection to reduce the variability involved with fluctuating particle penetration and to efficiently utilize the torches energy.

CTSR has also developed unique procedures to process and analyze sensor data. These methods help the scientist to better visualize and interpret what is actually happening during the spray process. These processes include:

- Filtering large amounts of sensor data.
- Designing process maps to visualize the effects that torch parameters have on any stage of the spray process, from in-flight particle temperature to coating modulus.
- Converting measured data (temperature, velocity, and diameter) into more descriptive parameters that incorporate individual particle characteristics (melting index, kinetic energy).
- Using histograms to display distributions for large amounts of data.
- Fitting equations to data distributions to determine characteristic coefficients.

2.1 Grit Blasting Procedure

Rubber gloves are worn during this procedure to reduce the contamination of dirt and oil from the skin to the sample. The sample is first cleaned with acetone by applying a small amount to a paper towel and rubbing both sides thoroughly. The sample is then placed into the grit blasting chamber and the air pressure set to the desired level, 40psi for aluminum substrates. The sample is evenly sprayed on both sides using long smooth strokes. When finished, the sample is removed from the chamber and immediately wrapped in paper towel to keep it clean.

2.2 Sensor Arrangement

The Accuraspray and DPV2000 sensors must be mounted securely to a table. The following experiments used an instrument table that consisted of a 3/8” sheet of aluminum with an array of threaded holes and four aluminum legs with adjustable feet.

This table must be leveled so that the any rotation of the sensor heads does not result in optical path vertical motion. The table orientation is parallel to the spray sample inside the exhaust hood. The robot holding the plasma torch must be programmed to go to a precise location and orientation where the measurements would take place. In the case for Accuraspray, a ruler is mounted to the nozzle of the spray torch whose centerline lies along its axis. The surface of the nozzle is taken as the reference plane, and measurements are taken along the direction of spray. The prime candidate for sensor location is the center of the spray plume where the particle-substrate impact occurs. This is where the particles will accumulate to build a coating. The alignment LEDs on the Accuraspray sensor head must be activated and made to line up with the axis of the spray torch, which is the vertical reference for measurements. Then the lights must be centered at 10 cm offset from the face of the nozzle, which is the spray distance chosen. The size and shape of the light on the ruler indicates whether the sensor head is at the correct 90 degree angle. The sensors were then fixed to the table via machine screws.

The procedure for the DPV2000 is almost the same. There is one extra step of centering the DPV2000's x-y stage before carrying out the aforementioned procedure. Multiple sensors arranged on this table require a greater number of positions to be taught to the robot but allows multiple measurements to be quickly taken during a spray run. This is excellent for cross comparison of sensor data.

2.3 Injection Optimization

Injection optimization involves recording a set of in-flight particle data from the diagnostic sensors while discretely varying the carrier gas flow. Figure 2.3-1 displays the results from an injection optimization experiment of Titania. Each condition represents a different carrier gas flow rate that directly determines the amount of plume penetration that the particles achieve. From these plots a temperature peak and a velocity peak were determined using a second order polynomial curve fit. The peaks correlate to a specific plume position that, for all experiments, is considered to be 'optimized'. It is the position

where the maximum amount of the plasma's energy is transferred to the particles [13]. The optimum position is unique for each different powder and nozzle configuration, and requires a different level of injection carrier gas flow in order for the particles to effectively penetrate the plasma plume. Injection optimization for YSZ is demonstrated in [26] using three diagnostic tools, including DPV2000. Particle injection is an important aspect of the thermal spraying procedure because it partially determines melting state and also coating microstructure [27, 28].

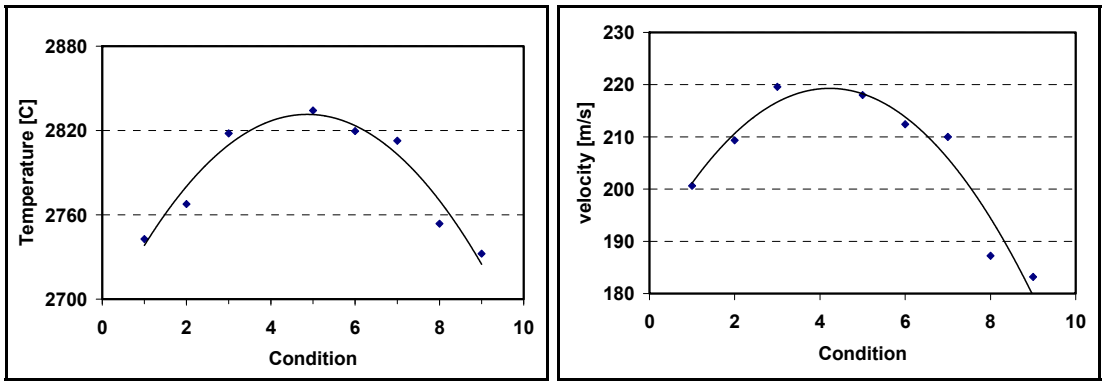

Figure 2.3-1. Injection optimization experiment using temperature (left) and velocity (right) as indicators to determine ideal carrier gas flow.

2.4 Factorial Design

A good experimental design is critical to any study where several input parameter combinations are possible. When operating the plasma torch, varying the ratio of the three input parameters results in different in-flight particle states and subsequently different coating properties. To determine the effects the three spray torch parameters, the factorial design process was followed [29]. In accordance with this design process, an experiment that has three input variables will require $n_1 \times n_2 \times n_3$ number of experiments to determine each variable's effect on the output parameter, where n_i is the number of discrete values for each particular variable. For example, if there are three input variables whose values can be either 'high' or 'low', then there is a need to run a

series of eight experiments ($2 \times 2 \times 2 = 8$), see Table 2.4-1. This ensures that all possible combinations of input variables are tested. Following the factorial design method enables the individual effects and combined/interactive effects to be extracted by interpreting the resulting data.

Condition	Argon (slpm)	Hydrogen (slpm)	Current [A]
1	H	H	H
2	H	H	L
3	H	L	H
4	H	L	L
5	L	H	H
6	L	H	L
7	L	L	H
8	L	L	L

Table 2.4-1. Factorial design table showing all of the unique combinations for a three parameter-two value system.

2.5 Elliptical Truncation

The DPV2000 is capable of measuring a high number of individual particles, typically between 5,000 and 10,000 for one diagnostic measurement. When a typical two dimensional plot of temperature vs. velocity is made from this data, a filtering method must be used in order to visualize the data coherently. Without filtering the data looks very scattered and without shape. The following filtering method of elliptical truncation takes a 10%-90% cut of the data that is contained within an ellipse. Shown below in Figure 2.5-1 is the diagram of an ellipse that was used as a reference when describing the truncation formula, Equation 4.

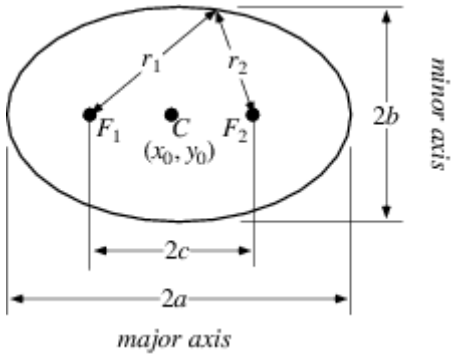

Figure 2.5-1. Ellipse showing the center, major axis, and minor axis. Image taken from http://mathworld.wolfram.com/Ellipse.html, June 2009.

$$\frac{(x-x_0)^2}{a^2}+\frac{(y-y_0)^2}{b^2}=1 \qquad \textbf{4}$$

x_0 = average x-parameter value (i.e. velocity)
y_0 = average y-parameter value (i.e. temperature)
x = x-parameter data (i.e. measured velocity values)
y = y-parameter data (i.e. measured temperature values)
a = ½ distance of major axis
b = ½ distance of minor axis

The following steps outline the procedure used: First a statistical box plot of the x-parameter data was made to show the 10%-90% distribution values. The range between these values was used as the major axis of the ellipse. Similarly, this procedure was done for the y-parameter data to determine the minor axis of the ellipse. The values for "a" and "b" were input into Equation 4. The x-parameter mean and y-parameter, x_0 and y_0, were calculated and input to Equation 4. The measured data was then tested against Equation 4. All data that did not satisfy the equation was rejected. The remaining data was in the form of an elliptical distribution whose position was based on the data's average measured value.

Shown below in Figure 2.5-2 is a demonstration of the elliptical truncation method on real sensor data taken from the DPV2000. The data came from a series of 12 spray conditions. The plot on the left was made from the raw data taken directly from the sensor's output file. Elliptical truncation was preformed on this set of data to obtain the plot on the right. It became clear that each spray condition had a unique shape and location on the TV space.

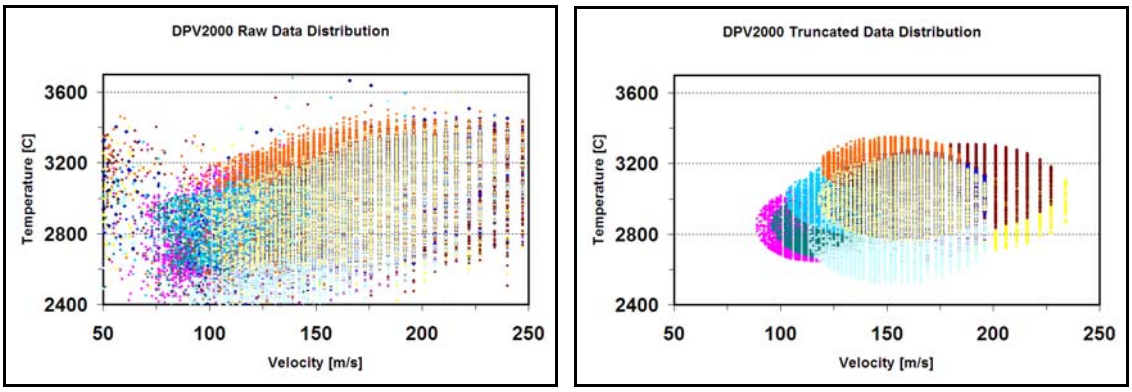

Figure 2.5-2. Temperature-velocity plots of entire process map before (left) and after (right) elliptical truncation. Data taken from DPV2000.

2.6 Grouped Parameters

Since the DPV2000 has the capability of measuring individual in-flight particle properties such as temperature, velocity, and diameter, its data was used to calculate grouped parameters that are more unique to each individual particle. These grouped parameters took into account the flight history and individual thermal and physical properties for each individual particle. The first grouped parameter, kinetic energy, was calculated as half the particle's mass times its squared velocity. The mass was calculated from the measured diameter and known powder density and geometry. The second grouped parameter, melting index, was calculated using a somewhat more complicated equation (Equation 5) derived previously in [28].

$$MI = \frac{\Delta t_{fly}}{\Delta t_{melt}} = \frac{24k}{\rho h_{fg}} \cdot \frac{1}{1+4/Bi} \cdot \frac{(T_f - T_m) \cdot \Delta t_{fly}}{D^2} \qquad \textbf{5}$$

Δt_{fly} = estimated time of flight of particle
Δt_{melt} = time for particle to fully melt
k = thermal conductivity of material
ρ = density of material
h_{fg} = enthalpy of fusion
Bi = Biot number of the particle
T_f = measured particle temperature
T_m = melting point of material

D = particle diameter

The melting index is a ratio between the amount of time the particle is in flight within the plasma and the amount of time required to fully melt the particle. Indirectly, it describes the percent of the particle that is in liquid state. The particle and plasma properties are condensed to form a quantitative "time to melt" property which is the time required for the particle to become fully molten. The particle's thermal and physical properties combined with the plasma environment determine the rate of heat transfer to the particle.

2.7 Histograms

Histograms are a very useful way to report large amounts of data when the average values do not sufficiently describe an experiments outcome. Histogram representation prevents the loss of value that occurs when data is oversimplified. Previous experiments show how the distribution of temperature and velocity measurements changes when moving to different conditions around the process map [30]. For the following experiments the bin width of the histograms was chosen according to Scott's formula [31], shown in Equation 6. This formula calculates the bin width based on the sample size and standard deviation of the measured data.

$$W = 3.49\sigma N^{-1/3} \quad \textbf{6}$$

W = Bin Width
σ = Standard deviation of the distribution
N = Sample size

The number of bins were calculated using the following formula:

$$k = \left\lceil \frac{\max x - \min x}{W} \right\rceil \quad \textbf{7}$$

k = Number of bins
x = Data value
W = Bin width

Shown below in Figure 2.7-1 is the histogram representation of temperature and velocity data measured by the DPV2000. The distribution shapes are unique to the powder feedstock-spray condition combination. The temperature distributions occasionally display a bi-modal characteristic. This occurs when a significant number of particles are at the melting temperature going through a phase transformation. This phenomenon vanishes as the torch's power increases and the particle's surfaces are fully molten. Velocity distributions are typically Gaussian and closely follow the shape of particle size distribution.

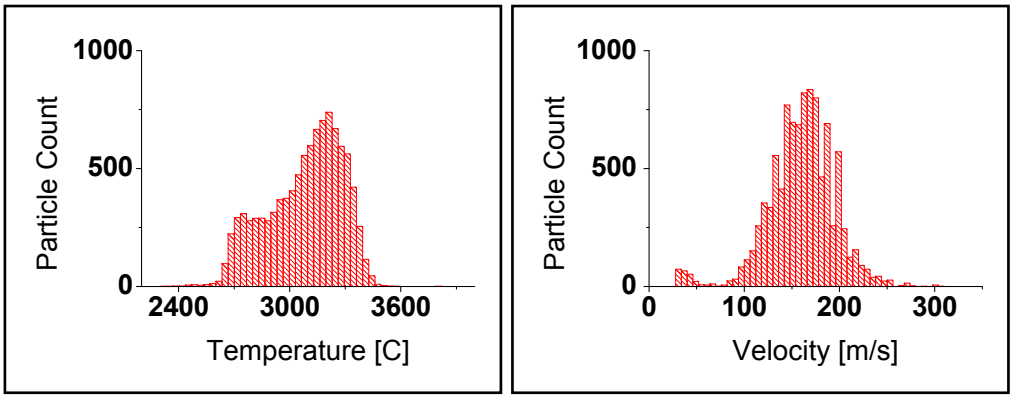

Figure 2.7-1. Example of histogram made from temperature and velocity data measured by the DPV2000. Bin sizes calculated using Scott's formula.

2.8 Bi-Modal Curve Fitting

The histograms typically follow either a normal Gaussian distribution or a bi-modal Gaussian distribution. In order to compare data distributions, a curve fitting method was developed making use of the general probability density function (PDF) and adapting it to accurately represent the data measured. The basic PDF is shown in equation 8.

$$P = \frac{1}{\sigma\sqrt{2\pi}} \exp\left(-\frac{(x-\mu)^2}{2\sigma^2} \right) \qquad \textbf{8}$$

P = probability that x will be found
σ = standard deviation
μ = mean

In order to fit the PDF to a histogram distribution, equation 8 must be scaled so that the probability values equals the number of particles measured for a particular histogram bin. So the modified PDF equation is shown in equation 9.

$$P = PC \bullet BS \frac{1}{\sigma\sqrt{2\pi}} \exp\left(-\frac{(x-\mu)^2}{2\sigma^2} \right) \quad \textbf{9}$$

PC = number of particles measured
BS = bin size

At this point, in order to fit normal distribution curve to the histogram, a series of discrete values of x are chosen to coincide with the bin locations of the histogram. The goal here is to minimize the sum-difference between the equation and the histogram values and attain a value for μ and σ.

For a bi-modal distribution a second modified PDF equation must be created that combines two normal PDFs, shown in equation 10. The scaling factor, *s*, is required to correctly distribute the particles to either PDF curve. This function is solved in the same fashion previously described for normal distribution curve fitting. Discrete values for x are chosen and the resulting value of the function is compared to the histogram value. The difference of these numbers is minimized to solve for the five variables.

$$P_{BiModal} = s \bullet PC \bullet BS \frac{1}{\sigma_1\sqrt{2\pi}} \exp\left(-\frac{(x-\mu_1)^2}{2\sigma_1^2} \right) + (1-s)\, PC \bullet BS \frac{1}{\sigma_2\sqrt{2\pi}} \exp\left(-\frac{(x-\mu_2)^2}{2\sigma_2^2} \right) \quad \textbf{10}$$

s: scaling factor

Shown below in Figure 2.8-1 is the result of a bi-modal curve fitting to temperature data that was measured by the DPV2000.

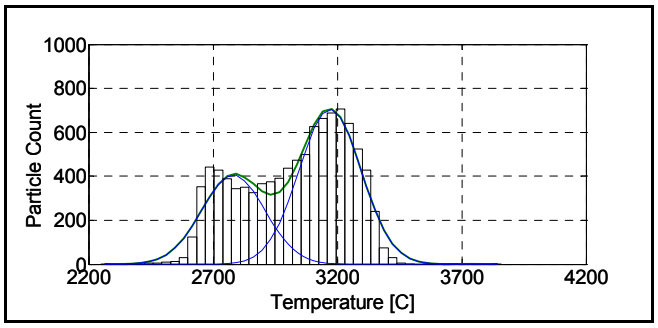

μ_1 [C]	σ_1 [C]	μ_2 [C]	σ_2 [C]	s
2782	128	3170	125	0.37

Figure 2.8-1. Example of bi-modal curve fitting using temperature data acquired from DPV2000. Bi-modal variables are shown.

3 Repeatability of Process Space

Process maps are used to link the plasma torch input parameters to a set of output states [13, 20, 32]. Process maps can be defined for various steps of the process. A first-order process map links the temperature and velocity of the injected powder to the torch's gas flows and current settings. Process maps are a good way for an operator or engineer to repeat an experiment with greater accuracy. Past experiments have shown that simply turning on the plasma torch and using the same spray conditions does not always lead to the same particle temperature and velocity, and furthermore the same coating [13]. By analyzing process maps, trends can be ascertained that help fine tune gun parameters to achieve a more stable and consistent T&V [32].

Second order process maps make connections of coating properties and microstructure to torch settings. These maps are more intuitive because, unlike the first order map that leaves the engineer somewhere in the middle of the spray process, the direct outcome of the coating is illustrated and the correct parameters that will achieve the desired property can be found [13, 20].

3.1 Procedures: Design of Process Map

The process map conditions of the following experiments were created based on the operational limits of the plasma torch. The variables of the process map were 'argon flow rate', 'hydrogen flow rate', and 'current'. Based on the method of factorial design, a combination of eight spray parameters are necessary in order to single out the effect of one variable, i.e. how an increase of current will affect T and V. The process maps in this paper also use a center condition that represents the typical torch parameters unique to each powder feedstock. The center condition was repeated four times within a process map, bringing the total number of conditions up to 12.

3.2 Procedures: Repeatability of Process Maps

A small amount of two powders were tested with a Beckman Coulter LS 13 320 Particle Size Analyzer to find their particle size distribution. The process maps were created over a period of several days and multiple hours of gun time. This is closely linked to how production parts are sprayed on different days and with a wearing nozzle/cathode, different ambient humidity/temperature etc. The powder feeder was cleaned with compressed air and the wheel cleaned with alcohol to eliminate any chances of contamination. The feeder hose was also blown with compressed air before each run to clear out any residual particles. The powder was added so that the hopper was about half full. A flow calibration was conducted by setting the powder feeder to a known velocity and catching the powder in a plastic bag for one minute. The goal was to achieve the same flow rate over each experiment, 2.0 g/m. After flow rate was set, the gun was turned on and gradually warmed up to the Design of Experiments (DoE) center condition. At this point the powder was turned on and the torch was moved to the Accuraspray sensor to find the correct setting of the carrier gas flow for the optimal injection of particles. After the injection was set, the sensor recorded data for 15 seconds before moving the torch to the DPV2000 sensor. The 'autocenter' feature was used in order to find position where the flux of particles was the highest. At this position, 5000 individual 'good' particles were measured and recorded. This procedure was repeated for

the remaining 11 conditions. The data collected was used to generate a first order process map by making a 2-D plot of the average temperature and velocity of each condition.

During the creation of a process map, the center condition was repeated four times at equal intervals. This applies to all YSZ HOSP 1 and YSZ HOSP 2 process map experiments. The purpose was to measure the variability of one condition without restarting the torch.

After generating a series of five process maps of YSZ HOSP 1 and YSZ HOSP 2 each over the course of one week, special attention was given to the variability of individual conditions of the process map. The temperature distributions of the tightest and widest repeated average temperature ranges were compared.

3.3 Analyzing Data

There are many ways in which to compare one thermal spray run to another. The experiments discussed in this paper limit the number of control variables to a minimum in order to focus on the data taken by the diagnostic equipment and ensure comparable results. Two primary characteristics of the in-flight particles measured directly by the sensors were temperature and velocity. These two characteristics are typically plotted against each other to create a 2-D map. From DPV2000 data, melting index-kinetic energy plots were made which take into account the physical condition of individual particles.

3.4 Results and Discussion: Repeatability of Process Maps

The results of the particle size analysis of the YSZ HOSP 1 are shown in Figure 3.4-1. The average particle size was found to be 56μm with 80% of the particles (10% to 90%) between 24μm and 95μm.

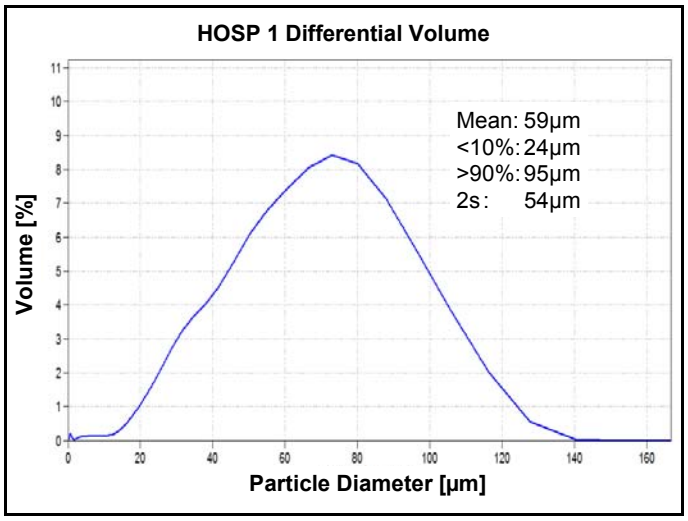

Figure 3.4-1. Particle size distribution of YSZ HOSP 1 measured by the Beckman Coulter LS 13 320 Particle Size Analyzer.

3.4.1 Average Temperature-Velocity and Data Distributions

Average TV values from each process map overlaid on the same TV space, shown in Figure 3.4-2, using the data measured by reveals some interesting characteristics about each spray condition. It can be seen that some conditions have a more tightly grouped set of average values. Condition 5, measured by DPV2000, has the lowest variability in both average temperature and average velocity with a 2σ deviation of only 29°C and 4m/s respectively. This condition was further investigated to test the effects that a 'tight' spray condition has on coating property variability. The other extreme case is condition 9 that has a 2σ deviation of 177 C and 18 m/s in temperature and velocity, respectively. For all cases, the average values and corresponding 2σ standard deviations are tabulated in Table 3.4-1.

Figure 3.4-2 also compares the average temperature and velocity data between two commonly used diagnostic equipment, DPV2000 and Accuraspray (Tecnar). Discrepancies between the two sensors became obvious when plotted side by side. The average values and distributions are not consistent. While condition 10 appears to be the hottest on Accuraspray, it is the coldest on DPV2000. It can be seen that the DPV2000 recorded a smaller temperature range of the entire process map (486°C) than the

Accuraspray (1190°C). This discrepancy was also found in the process map velocity range, being 94m/s on the DPV2000 and 79.5m/s on the Accuraspray.

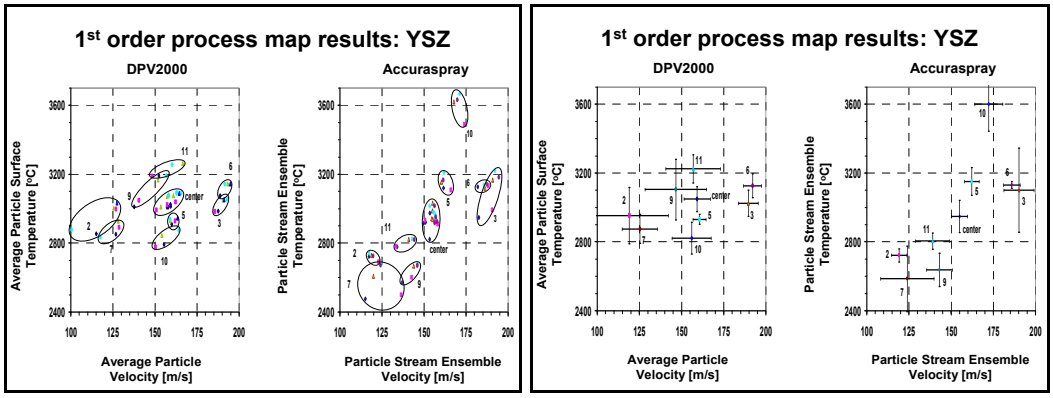

Figure 3.4-2. Average TVs (left and right) with 2σ standard deviations (right) from five first order process maps of YSZ HOSP 1 measured by DPV2000 and Accuraspray.

	Average		2σ Deviation	
Condition	T [C]	V [m/s]	T [C]	V [m/s]
1	3049	159	73	8
2	2953	119	164	23
3	3025	190	75	6
5	2931	161	29	4
6	3127	192	69	5
7	2876	125	84	10
9	3104	147	177	18
10	2822	156	92	12
11	3224	157	81	16

Table 3.4-1. List of statistical data from the series of five YSZ HOSP 1 process maps. Each condition has a unique average TV and 2σ standard deviation. Conditions 4, 8, and 12 are contained within condition 1 due to repeated torch settings.

When measuring individual particles, a look at the data distributions reveals some interesting facts about the particle spray stream that is not possible to see by looking only at average values [13, 33]. A spray condition may result in the same average T&V but may have completely different distributions of data [34]. A deeper investigation of the process map data from a single map reveals different ranges of individual particle TV measurements for each of the unique process conditions, shown in Figure 3.4-3. Not much can be inferred from the raw data plot of temperature and velocity except for the boundaries of the TV space. A 10-90% elliptical truncation was performed in order to filter the data and capture the particles that would most significantly contribute to coating production. It can be seen that each condition has a unique position and unique shape

that represent its collection of particle states. The position of each point cloud represents the average calculated from the original raw data, and the shape of the cloud represents the distribution of measurements. If many measurements overlap within a confined region of TV space, the point cloud appears small and dense. This situation results from the data having a small standard deviation. Conversely, if the point cloud covers a wide area of TV space and appears less dense there is a large standard deviation of the data and a broader distribution of particle states. These different distributions of particle states may have a critical impact on coating properties and performance.

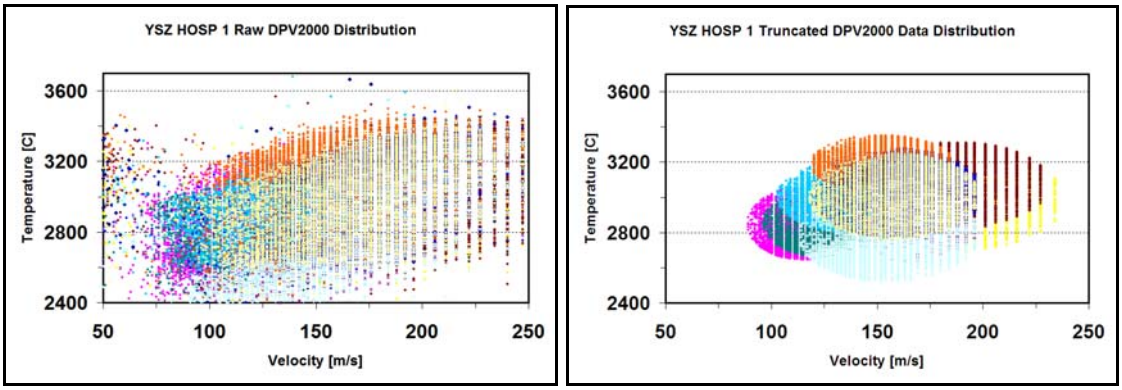

Figure 3.4-3. Temperature-velocity plots of entire YSZ HOSP 1 process map before (left) and after (right) elliptical truncation. Data taken from DPV2000.

A set of temperature and velocity histograms were created for all the conditions of a single process map, shown in Figure 3.4-4 and Figure 3.4-5. Both sets histograms are arranged in order of increasing average temperature, beginning on the bottom left and ending on the top right. Histogram representation of TV data improves the clarity of measurement density, when there are repeated points that overlap on the TV space. In these histograms the x-axis is the property being measured and the y-axis is the particle count. The shape of the temperature histogram is typically bi-modal, with particles accumulating at the melting point of the powder, unless the plasma energy is high enough to sufficiently melt the particle surface. The narrowest distribution of temperature occurred in Condition 7 with a standard deviation of 160 °C, followed by Condition 11 with a standard deviation of 163 °C. These two conditions had a narrow band of temperature with a high particle count. Conversely, the widest distribution of

temperature occurred in Condition 10, with a standard deviation of 235 °C, and in Condition 5, with a standard deviation of 234 °C. These conditions cover a broader band of temperature with a lower particle count at any given point. The bin size of these conditions is larger because Scott's formula for bin size is a function of the data set's standard deviation. The statistics of each histogram are listed in Table 3.4-2.

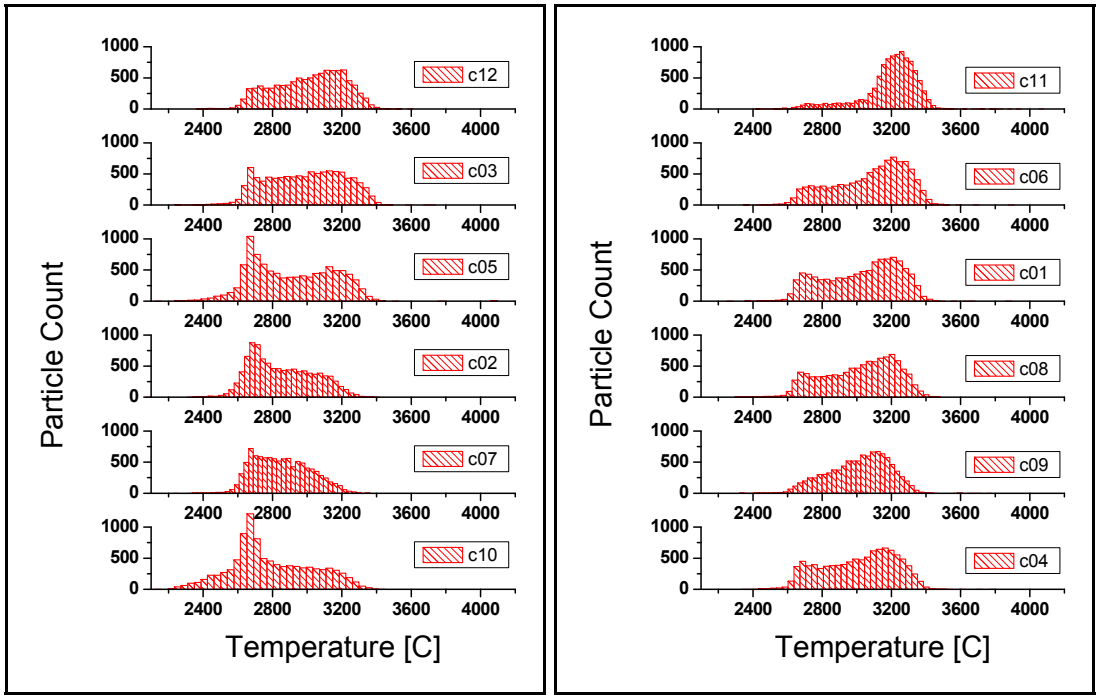

Figure 3.4-4. Temperature distributions for each condition of YSZ HOSP 1 process map. Scott's formula was used for bin sizing. Plots are arranged in order of increasing average temperature beginning at bottom left and ending at top right.

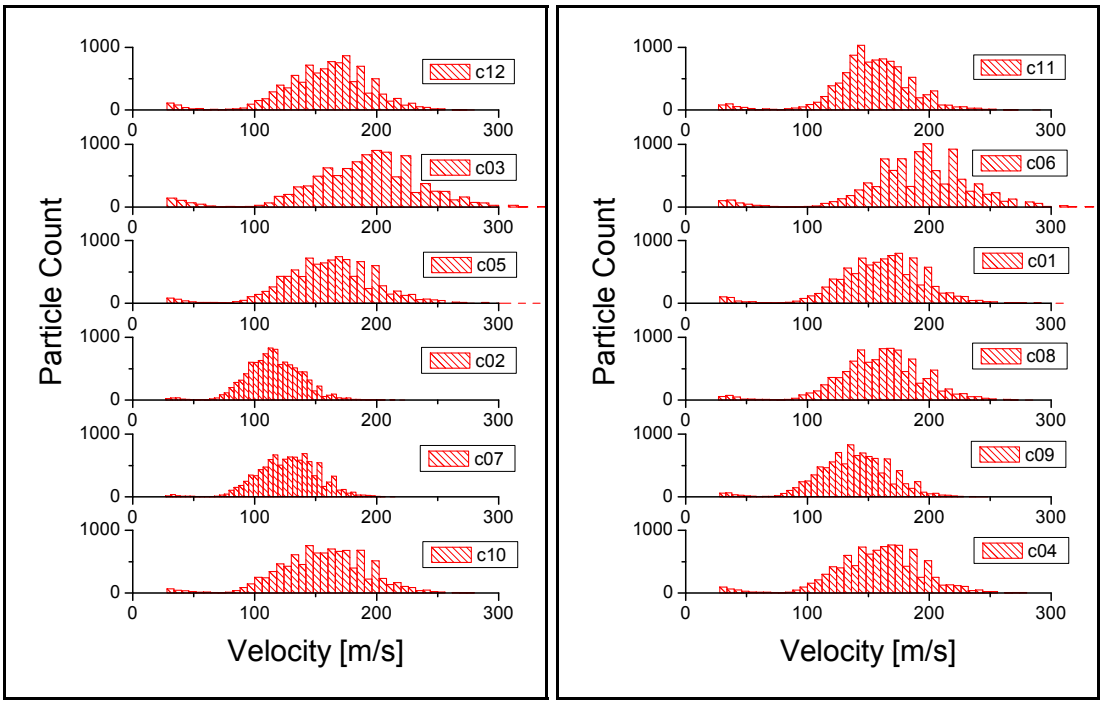

Figure 3.4-5. Velocity distributions for each condition of YSZ HOSP 1 process map. Scott's formula was used for bin sizing. Plots are arranged in order of increasing average temperature beginning at bottom left and ending at top right.

Condition	T Average [C]	T Standard Deviation [C]	T Bin Size [C]	V Average [C]	V Standard Deviation [C]	V Bin Size [C]
1	3025	214	35	159	37	6
2	2854	183	30	115	23	4
3	2985	217	35	188	48	8
4	3009	209	34	157	36	6
5	2908	234	38	160	38	6
6	3075	209	34	189	46	7
7	2853	160	26	127	25	4
8	3014	207	33	159	36	6
9	3011	173	28	138	31	5
10	2792	235	38	155	36	6
11	3190	163	26	152	34	6
12	3008	197	32	158	37	6

Table 3.4-2. Statistics of TV histograms for YSZ HOSP 1, calculated from DPV 2000 data. Bin sizes calculated using Scot's formula that is directly related to the standard deviation.

3.4.2 Tight and Wide Average TV

Condition 5 and condition 9 were considered to be the most extreme cases of high and low variability in terms of average TV, based on standard deviation. A closer look at

their temperature distributions compared over the five process map runs is shown in Figure 3.4-6. For the tightest condition, c05, the temperature distributions are almost identical. The average temperature, which indicates the location of the distribution, throughout the five runs varies within a range of only 38 °C. On the contrary, for the widest condition, c02, the temperature distributions are clearly different. The average temperature range is much larger, 182 °C. These statistics are listed in Table 3.4-3.

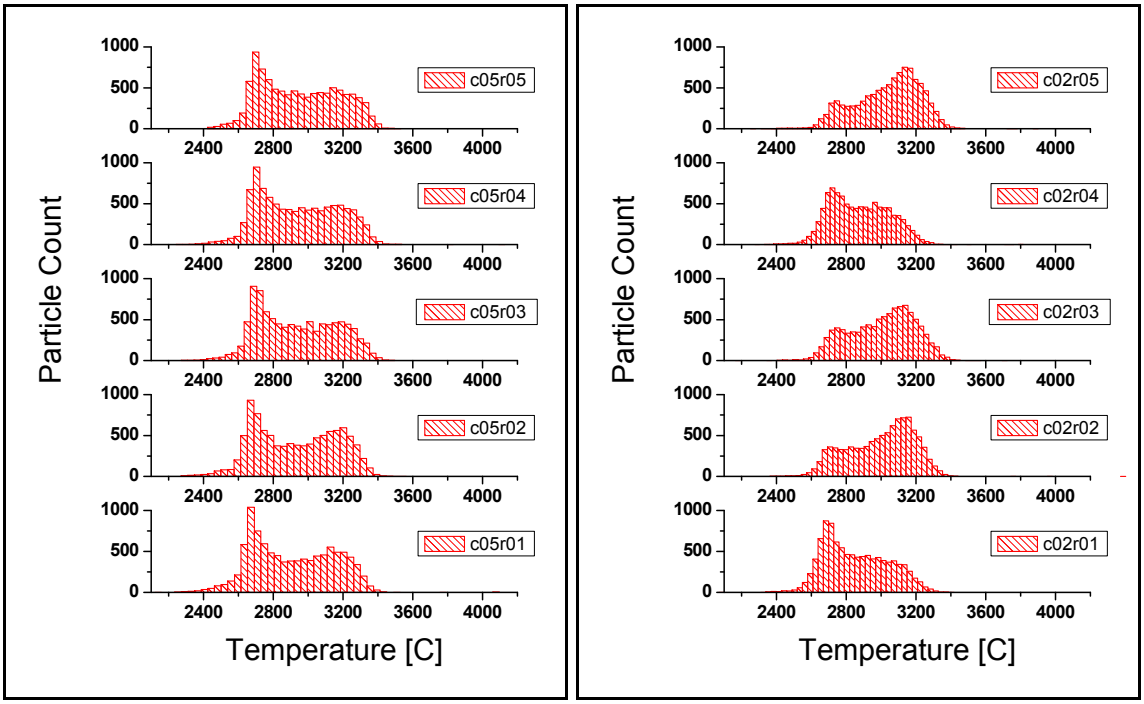

Figure 3.4-6. YSZ HOSP 1 temperature distributions for tight (c05 on left) and wide (c02 on right) conditions over five process maps.

	Condition 5		Condition 2	
Run	T avg [C]	T 2σ [C]	T avg [C]	T 2σ [C]
1	2908	234	2854	183
2	2928	233	2996	187
3	2933	223	3003	186
4	2939	226	2877	170
5	2946	227	3035	183
Range	38	11	182	17

Table 3.4-3. Statistics of Condition 5 and Condition 2 histograms calculated from five repeated process maps.

3.4.3 Melting Index-Kinetic Energy Maps

A question has been raised if T&V are sufficient descriptors of the in-flight particle state and if other characteristics could be useful [33]. This lead to the development of two parameters, 'melting index' and 'kinetic energy', that are characteristics of individual particles and account for their physical properties. The melting index describes what percent of the particle has been melted at the point where the particle impacts the substrate [13]. It takes into account the particle's temperature, its volume, its time of flight, and its Biot number. The kinetic energy was also calculated at the impact site between particle and substrate. The kinetic energy is equal to half the mass times the squared velocity. The mass was calculated from the powders density and the particle's volume. The particles volume was calculated using the DPV2000's measurement of diameter. The raw data conversion from DPV2000 is shown in Figure 3.4-7. It can be seen that the melting index has both positive and negative values. This suggests that some of the particles are not melted (MI<0) and some are partially melted (0<MI<1). When a 10%-90% elliptical truncation was preformed, it became clear that the majority of the particles were in the partially melted zone. An important observation was that one group of particles showed a significantly higher MI than the others. This group corresponds to the DoE 'condition 11' which had a low argon flow, high hydrogen flow, and high current torch settings. Looking back at the DPV2000 TV space in Figure 3.4-2, this was the condition that had the highest temperature combined with a medium velocity compared to the other DoE conditions. High temperature and low velocity created a better situation for heat transfer because the high temperature drove more heat into the particle faster while the low velocity allowed the particle more time to absorb it.

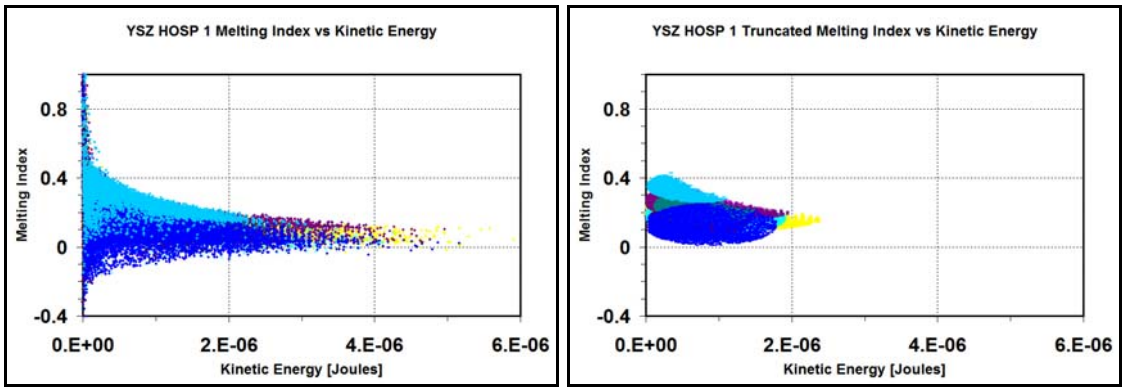

Figure 3.4-7. YSZ HOSP 1 MI-KE plots of raw data (left) and truncated data (right) calculated from DPV2000 data.

Histograms of melting index and kinetic energy are shown below in Figure 3.4-8 and Figure 3.4-9. They are arranged in increasing order of average melting index, from lower left to top right. Since the melting index is directly related to the particle temperature, some of the MI histograms also displayed a bi-modal distribution. But, the bi-modal distributions were not so profound in MI due to the consideration of each particle's size. Again, there is an accumulation of data on the low end of the scale, between zero and 0.5, suggesting a mostly un-melted particle. Each condition's data displayed its own unique location and shape on the histogram. These locations and shapes are believed to have a direct influence on coating property variations.

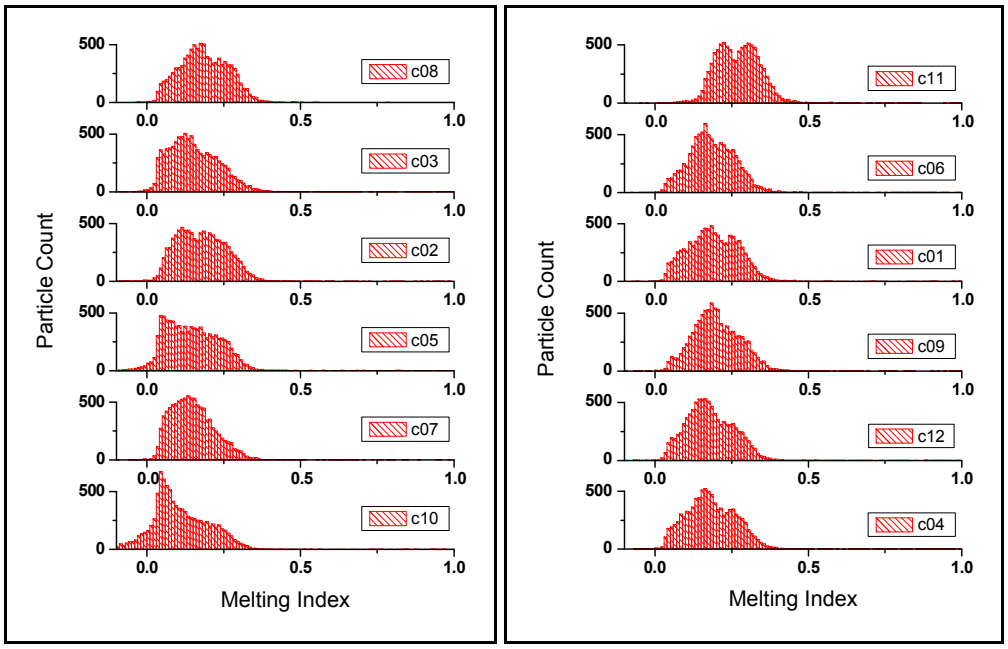

Figure 3.4-8. MI distributions for each condition of YSZ HOSP 1 process map calculated from DPV2000 data. Plots are arranged in order of increasing average melting index beginning at bottom left and ending at top right.

The kinetic energy histograms displayed new distributions that closely represent half-Gaussian curves with a center at zero. This was an interesting observation since the distribution of velocity was full Gaussian. The individual kinetic energies measured during this process map ranged between $1x10^{-10}$ J and $7x10^{-6}$ J.

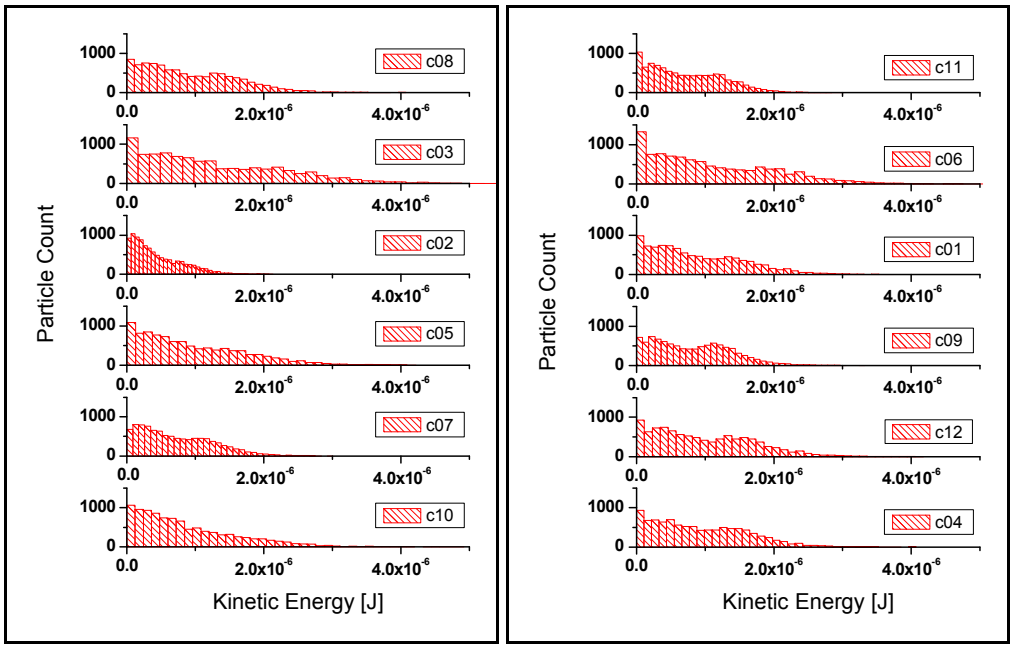

Figure 3.4-9. KE distributions for each condition of YSZ HOSP 1 process map. Scott's formula was used for bin sizing. Plots are arranged in order of increasing average melting index beginning at bottom left and ending at top right.

Condition	MI Average	MI Standard Deviation	KE Average [J]	KE Standard Deviation [J]
1	0.24	0.37	8.8E-07	6.6E-07
2	0.20	0.21	4.4E-07	3.7E-07
3	0.22	0.41	1.3E-06	1.0E-06
4	0.23	0.33	9.3E-07	6.8E-07
5	0.18	0.29	9.6E-07	7.6E-07
6	0.26	0.46	1.1E-06	8.9E-07
7	0.16	0.14	7.3E-07	5.3E-07
8	0.22	0.29	9.2E-07	6.8E-07
9	0.24	0.29	8.1E-07	5.6E-07
10	0.13	0.24	8.7E-07	7.3E-07
11	0.35	0.49	7.2E-07	5.3E-07
12	0.23	0.35	9.9E-07	7.2E-07

Table 3.4-4. Average MI and KE values with their standard deviations of YSZ HOSP 1 calculated from DPV 2000 data.

3.5 Conclusions:

Process map design is an important step to ensure that the full range of gun parameters is utilized. This allows the torch operator or engineer to foresee the broadest range of desired particle states, in the case of a first order map, for any combination of spray parameters and choose accordingly. The factorial design allows the individual effects of torch parameter changes to be determined by recording and analyzing data for each combination of spray parameter.

Repeating measurements of the entire process map lead to some interesting observations. Each spray condition had its own unique variability of average temperature and velocity measurements when repeated over a series of five process maps. Also, unique distributions were found during the measurement of individual particle data at each condition. By looking at these maps of repeated data, a spray condition can be chosen not only by its position in the TV space but also by its TV distribution. Further studies were focused upon comparing the coatings made by each of the spray conditions. The hypothesis is that the coatings made by the tighter spray conditions will have lower coating property variability.

An interesting observation was made as a result of plotting the individual TV particle data. As the particles measured by the DPV2000 became faster, the space between recorded values of velocity become larger. For example, the smaller values of velocity were reported every 1m/s where as the higher values of velocities were reported as much as 12m/s apart. This leads to error in any calculations made using the velocity values. This also leads to error when trying to repeat a spray condition, especially when there is a tight window of acceptable properties.

Considering the wide distribution of particle geometry (size, shape, and mass) that is encountered within a single spray run, temperature alone does not give enough information about what is going on within that particle. It is simply the surface temperature at the time of measurement. The same surface temperature measured from a large particle and a small particle does not accurately explain the extent to which the

particle is melted. These two particles clearly contain different amounts of thermal energy based on size (mass) and contribute different amounts of mass to the final coating. The 'melting index' takes into account the mass and volume properties attributed to each particle to predict their melting state. When combined with kinetic energy, it can directly predict particle impact characteristics, such as flattening ratio, and coating properties. It was important to measure MI and KE variability, considering how close they are tied to coating formation. A reduction in MI and KE variability will lead to a reduction in coating property variation.

4 Linkage of Particle States to Coating Properties

The following experiments measured the variability of in-flight particle states and coating properties of the same condition sprayed over five consecutive days. The term 'same condition' means that the torch input parameters (argon flow rate, hydrogen flow rate, and current) were fixed. Ensemble and individual particle in-flight diagnostics were taken immediately before each coating deposition by the Accuraspray and DPV2000 sensors. From both sets of data, the average TV variability was calculated. The TV distribution variability was calculated using the individual particle data from the DPV2000. The individual particle data was also used to calculate melting index and kinetic energy for each run. The average MI-KE variability and MI-KE distribution variability was also calculated.

Coatings were deposited on a 9"x1"x0.125" 6061-T6 aluminum substrate while recording substrate temperature and deflection with the ICP sensor's contact thermocouples and linear displacement laser. From these measurements the evolving stress, thermal stress, residual stress, and elastic modulus was calculated [19]. Post spraying, the thicknesses and weights of each sample were recorded and compared. The thermal conductivity of three randomly chosen samples was measured using laser flash technology. The thermal conductivity was used as a comparative measure of the coatings interlamellar bonding and porosity [3].

4.1 Procedures: Substrate Preparation and Spraying

The ICP sensor was turned on and allowed time to warm up until the laser and thermocouple readings stabilized. The aluminum substrate was prepared for the experiment by cleaning and grit blasting both surfaces with 60 grit silicon oxide sprayed at 40 psi (see grit blasting section in appendix). The sample's thickness and weight was measured before the coating was sprayed. The thickness was measured in five places, shown in Figure 4.1-1, and then averaged. The substrate was then brought to the spray booth. The lens of the ICP sensor was cleaned before each spray run with a cotton swab and alcohol. Two clips were attached to holes at the end of the substrate that allowed it to bend freely and it was loaded into the ICP sensor. After setting the plasma torch to the chosen spray parameters, the substrate was preheated with two passes of the torch, the powder feeder was started, and data was recorded while coating the substrate with a series of fifteen passes. The substrate was cooled by air jets with constant flow (front and back) during coating deposition. After the fifteen passes were completed, the torch was shutdown and the sample was allowed time to cool to room temperature.

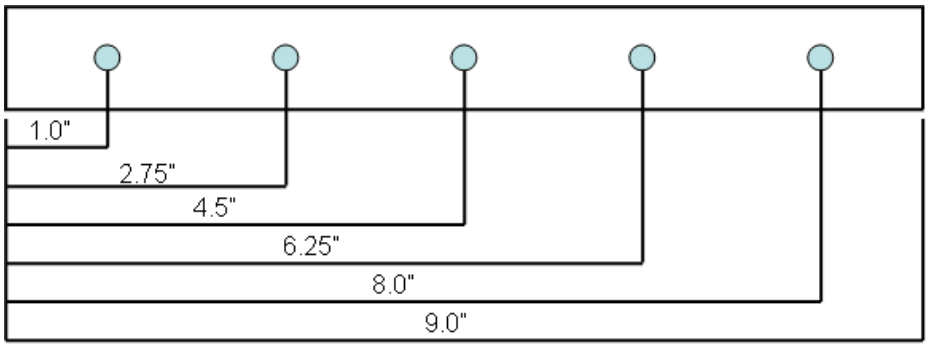

Figure 4.1-1. Location of thickness measurements for ICP substrate

4.2 Procedures: Thermal Conductivity

The thermal conductivity of a thermal spray coating is a good indicator of its porosity and splat to splat bonding, since they both affect the heat transfer through the coating [3]. The thermal conductivity of each coating was tested and compared using the following procedure: A small sample of the coating was removed from the substrate. This was done by first cutting off a small section of the knife sample (coating and substrate) with a circular diamond saw. The knife sample was placed in the saw so that the coating was facing the blade and would be cut first. This prevented pulling and contamination of the coating. An aluminum block was heated on a hot plate and small amount of wax was melted on its surface. The sample was placed coating side down into the wax, and then removed from the heat to cool in a water bath. The aluminum substrate was polished until only a thin layer remained, about 100μm. The remaining substrate was pealed off using needle nose pliers, leaving only the coating stuck in the wax. The block was then reheated to melt the wax and the coating was removed, cleaned in acetone, and allowed to air dry. In order for the coating to fit into the test machine, a Holometrix μflash (Netzsch Instrument Inc.), it needed to be shaped into a small 12.5mm diameter disk in order to fit into the sample fixture. The coating was cut with an ultra-fast laser using a precision computer controlled stage. This greatly reduced the variability in shape due to human error caused by hand polishing the sample into the disk shape. The disk samples were weighed and their dimensions were measured in order to calculate volume and density. The disk samples were then coated with graphite on both sides in order to enhance their light absorbing and emitting properties. Each sample's thermal conductivity was measured twice on each side.

4.3 Results and Discussion: Linkage of Particle States to Coating Properties

This experiment went one step past reporting the repeatability of only the process map TV by investigating the repeatability of coating properties when YSZ was deposited

on the ICP sensor. A total of 10,000 particles were measured by the DPV2000 before making each sample. The raw data was truncated using the elliptical method, shown in Figure 4.3-1. The truncated data from each spray run all have the same basic shape and location in TV space. They show only a slight shift in the point cloud, representing a small change in the average T&V.

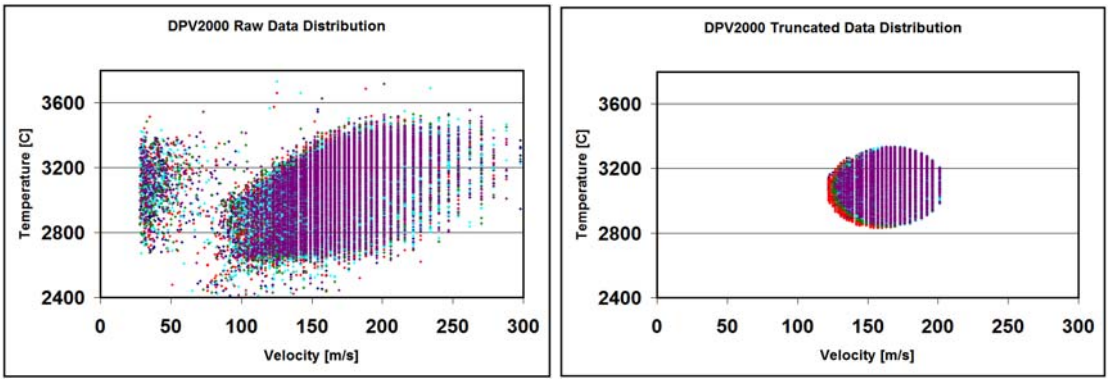

Figure 4.3-1. Raw (left) and truncated (right) DPV2000 TV data for 10,000 particles for each sample.

Average values of TV, calculated using data from both DPV2000 and Accuraspray, are shown in Figure 4.3-2. The range of data taken by each sensor was not consistent. The DPV2000 shows a range of 22 C and 9 m/s, while the Accuraspray shows a range of 44 C and 2 m/s.

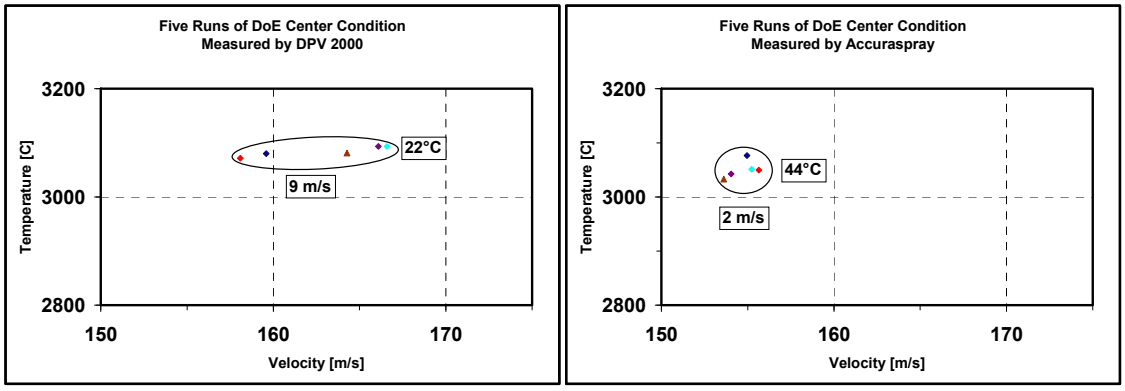

Figure 4.3-2. Average T&V for each sample measured by DPV2000 (left) and Accuraspray (right).

The temperature and velocity histograms in Figure 4.3-3 were created to visualize the difference in their distributions. Scott's formula was used for bin sizing because it consistently calculates a bin size relative to each data set's standard deviation and number

of measured particles. Each bar on the histogram represents the number of particles within that bin. The shapes of the temperature distributions are all very similar. They all show consistent peaks of particle count close to 2250 C and 175 m/s. The range of average TV was found to be only 23 C and 9 m/s, respectively. The sensor data statistics are shown in Table 4.3-1.

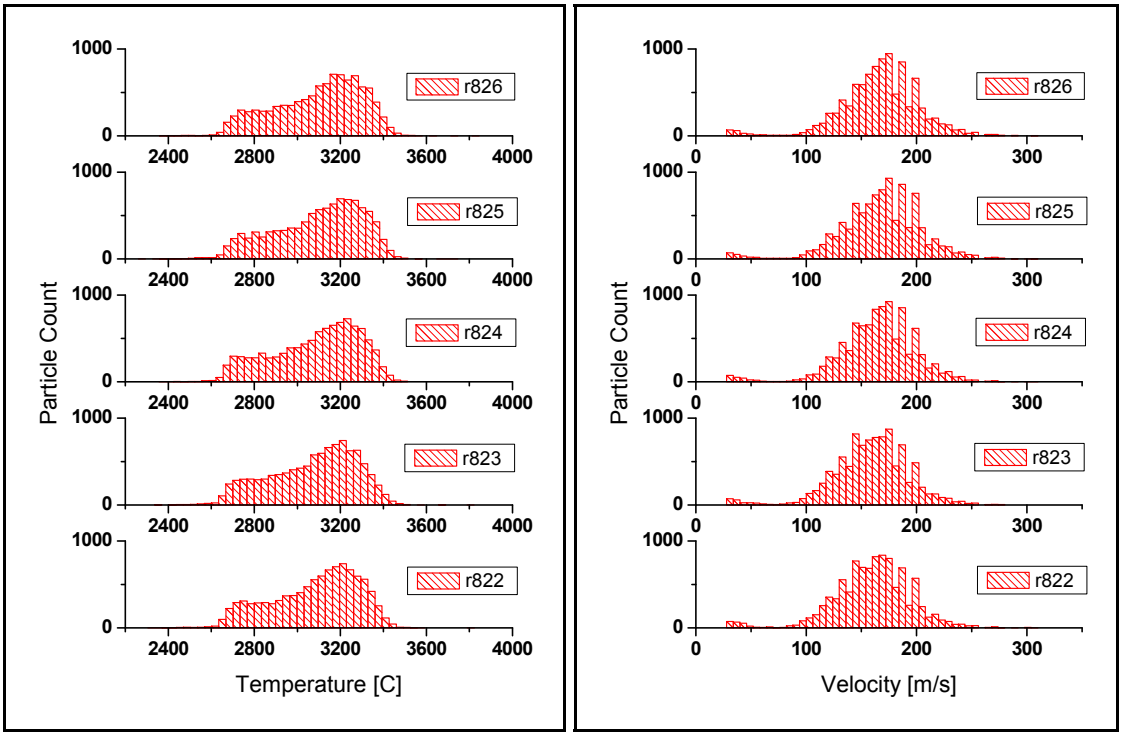

Figure 4.3-3. T and V distributions for each ICP coating measured by DPV2000.

Run	T Average[C]	T Standard Deviation [C]	V Average[m/s]	V Standard Deviation [m/s]
822	3080	201	159	35
823	3071	201	158	34
824	3083	203	164	35
825	3094	204	167	36
826	3094	201	166	35
Range	23	3	9	2
% change	0.74	1.63	5.30	5.60

Table 4.3-1. Average and standard deviations of temperature and velocity for each coating's in-flight particle diagnostic measured by DPV2000. Range of average values and standard deviations shown in bottom row.

Figure 4.3-4 presents all of the DPV2000 data converted to Melting Index and Kinetic Energy (MI and KE). The shape and position of the truncated point clouds nearly overlap between the five runs. The melting index and kinetic energy histograms, shown in Figure 4.3-5, are consistent in location and shape. Average MI-KE values and

standard deviations are shown in Table 4.3-2. The range of these properties varies only slightly, 0.009 for melting index and 4.12×10^{-8} J for kinetic energy.

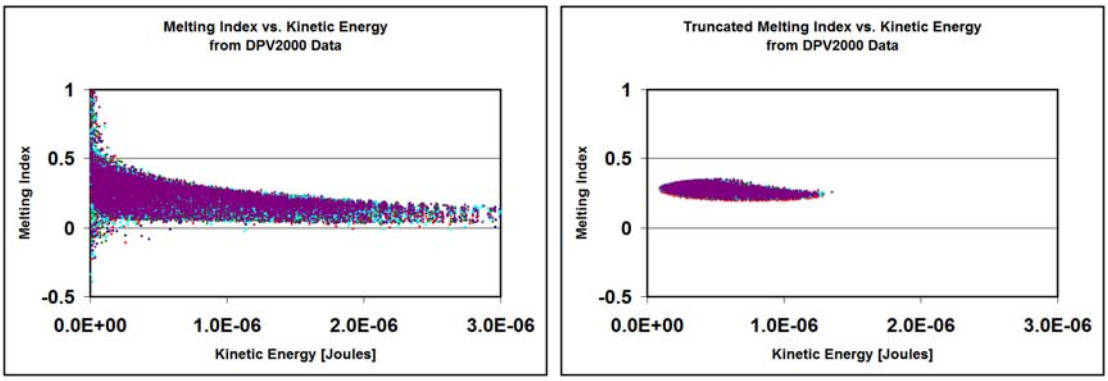

Figure 4.3-4. Raw (left) and truncated (right) data from DPV2000 converted to Melting Index and Kinetic Energy.

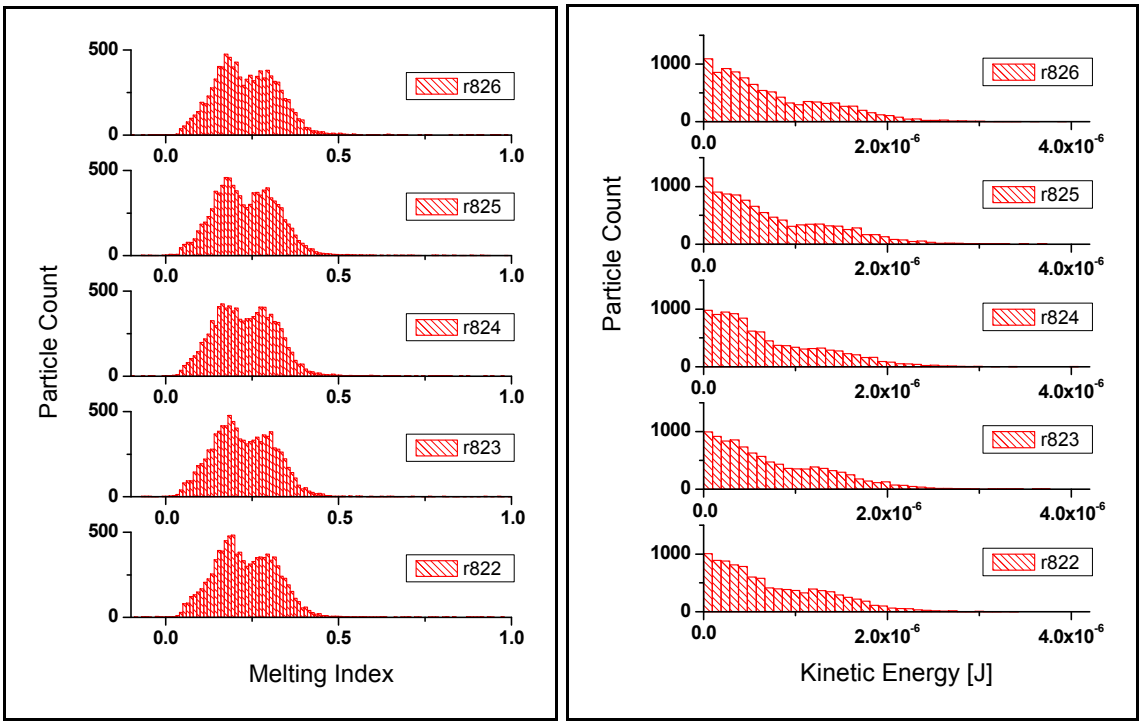

Figure 4.3-5. Melting index and kinetic energy distributions for each ICP coating calculated from DPV2000 data.

Run	MI Average	MI Standard Deviation	KE Average[J]	KE Standard Deviation [J]
822	0.280	0.384	7.35E-07	5.88E-07
823	0.273	0.384	7.45E-07	5.97E-07
824	0.279	0.380	7.13E-07	5.85E-07
825	0.283	0.400	7.54E-07	6.24E-07
826	0.282	0.381	7.45E-07	6.09E-07
Range	0.009	0.020	4.12E-08	3.83E-08
% change	3.27	5.22	5.58	6.38

Table 4.3-2. Statistics of melting index and kinetic energy for each run calculated from DPV2000 data.

The thickness per pass of each sample varied only slightly by 3.00µm. This value was calculated by taking the total measured thickness and dividing it by the number of passes. Although the maximum difference in coatings was only 3.00µm per pass, after 15 passes this resulted in a total thickness difference of 45µm which can significantly contribute to the stress state and elastic modulus of the coating. Using software developed at CTSR Stony Brook, a series of stress characteristics were calculated. The evolving stress is a measure of how the stresses develop during the spraying process as particles impact the substrate. The thermal stress of the coating is a result of the difference in thermal expansion between the two different materials. The residual stress is the final state of stress of the coating when it has cooled to room temperature. The stress values for each coating are shown below in Table 4.3-3.

Run	Thickness [µm]	Coating Passes	Thickness per Pass [µm]	Evolving Stress [MPa]	Thermal Stress [MPa]	Residual Stress [MPa]	Elastic Modulus [GPa]
822	653	20	32.64	21.9	-49.9	-25.4	25.4
823	488	15	32.53	17.4	-49.7	-34.8	19.1
824	516	15	34.40	14.1	-38.1	-30.6	15.3
825	471	15	31.40	14.4	-45.7	-33.3	17.1
826	493	15	32.86	18.8	-47.4	-28.1	21.6
Range			3.00	7.80	11.8	9.4	10.1
% Range			9	45	26	31	51
Standard Deviation			1.07	3.24	4.83	3.81	3.96

Table 4.3-3. Table of coating characteristics from repeated fixed condition spray runs.

The results of the thermal conductivity measurements are shown below in Figure 4.3-6. The thermal conductivity of each sample was measured by a Holometrix µflash

(Netzsch Instrument Inc.). The range of conductivity measurements from the first side was only 0.057W/m^2, about a six percent change. The second measurement of the r826 sample was significantly different from the others and considerably close to the first measurement. This might be due to making the error of measuring the same side twice.

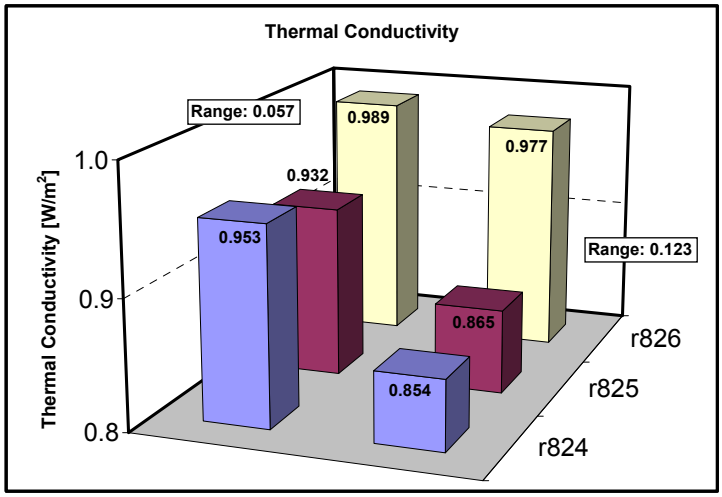

Figure 4.3-6. Thermal conductivity of three samples, r824, r825, and r826.

Since the spray runs from this experiment were conducted within one week, there was not much time for the torch's cathode and nozzle to wear considerably. When these runs were compared to a set of sensor data taken from the exact conditions measured two months earlier, a difference of 70 C and 4 m/s was found in average temperature and average velocity (truncated TV distributions shown below in Figure 4.3-7).

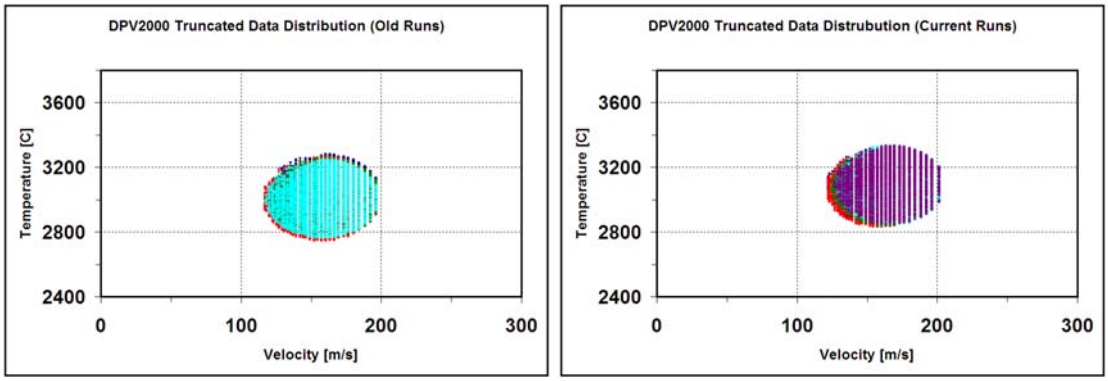

Figure 4.3-7. Comparison of repeated fixed condition spray run sensor data at different stages of cathode and nozzle wear. The plot on the left was created from data collected two months prior to running the current experiment (right). There was a change in average TV by 70 C and 4 m/s.

4.4 Conclusion: Linkage of Particle States to Coating Properties

Using all of the meticulous thermal spraying techniques of CTSR, a series of coatings were made on the ICP sensor. These methods followed pay close attention to the consistency of sample preparation and spray procedure. They represent the best case scenario to create a repeatable coating while minimizing the possibility of experimental error without the use of feedback control. Over these series of experiments the in-flight particle's temperature, velocity, melting index, and kinetic energy along with the thickness of each coating were tracked. These important characteristic play a critical role in the coating's residual stresses and elastic modulus.

The sensor data was reported in a number of different ways for clarity. The different representations of data were important because all information cannot be seen when simplifying results for a chart. While point clouds show the distribution shapes of two correlative characteristics they cannot accurately represent repeating data. Average values incorporate these repeated data and provide a locating parameter for data distributions. Histogram representation was used here to show the frequency of particles vs. one specific characteristic.

The small variability of both in-flight particle data and coating properties was partially contributed to the short time span in which these experiments were run. The cathode and anode of the plasma torch are in nearly the same condition for each run. If the experiments were carried out with longer intervals between spray runs, the wear on the plasma torch would affect the properties considerably. This concept was illustrated in Figure 4.3-7 and will be elaborated in the following section.

Although a difference of 3μm per pass does not appear to be significant, a total of 15 passes sprayed resulted in a difference of 45μm in coating thickness. This was enough to cause a difference in the final stress state and elastic modulus of the coatings. The values reported for stress states and elastic modulus were calculated using software

developed at CTSR. The software provided a consistent way of calculating these values given the data collected by the ICP sensor.

5 Effect of Hardware Degradation on Particle State and Coating

Over many hours of plasma torch operation, the cathode of the torch continuously wears and becomes less efficient. The tungsten from the cathode tip erodes causing the need for periodic replacement. This study investigated the effects of a cathode change by comparing sensor diagnostics and coating properties. The spray conditions were fixed to one value for both old and new cathode runs. Average TV and average MI-KE along with their relative particle distributions were investigated using data from both DPV2000 and Accuraspray sensors. Coatings were deposited on 6061-T6 aluminum substrates, dimensions 1"x9"x0.125", using the same number of passes and same powder feed rate. Coating thickness was measured as a means to compare deposition efficiency.

5.1 Procedures: Effect of Hardware Degradation on Particle State and Coating

A series of five process maps were created using an old worn cathode, with about three months of operating time on it, while measuring the in-flight particle TV with the DPV2000 sensor. The cathode was then replaced with a new unused one. Another process map was created using all of the same conditions as the previous maps. All the procedures for making a proper process map were followed during this experiment (injection optimization, consistent powder feed rates, etc.) The average TV values from each process map were compared.

The effect of a cathode change on a single condition (center of DoE) was analyzed in more detail. The condition was repeated five times before and after replacing

the cathode while recording sensor data from Accuraspray and DPV2000. Distributions from the DPV2000 TV data were created and compared. DPV2000 data was used to calculate MI-KE distributions for each spray run.

Three coatings were made on 6061-T6 aluminum substrates using low, medium, and high energy DoE spray conditions. Before each coating, an in-flight particle diagnostic was performed using the DPV2000. The cathode change effect on all three conditions was compared by means of average TV and coating thickness.

5.2 Results and Discussion: Effect of Hardware Degradation on Particle State and Coating

Figure 5.2-1 shows the average values of T and V from a series of five old-cathode process maps and one new-cathode process map. The old cathode data is displayed as the average TV and 2σ standard deviation calculated from the five spray runs. Most of the new cathode data fell within the 2σ bars with the remaining points very close by. There was a slight increase in all temperature values.

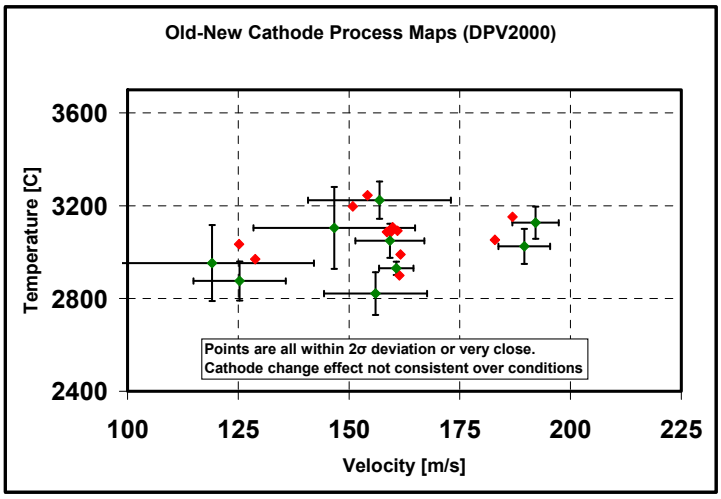

Figure 5.2-1. Overlapping process maps displaying the effect of a cathode change.

Figure 5.2-2 shows data taken by Accuraspray and DPV2000 while spraying a series of DoE center conditions. The effect of changing the cathode was clearly seen here

due to the grouping of same condition data points. The two sensors showed different but significant results. According to Accuraspray, changing the cathode caused the average temperature to drop by 95.2°C and the average velocity to decrease 2.6m/s. On the other hand, the average temperature measured by DPV2000 increased by 6.8°C while the average velocity decreased by 8.1m/s.

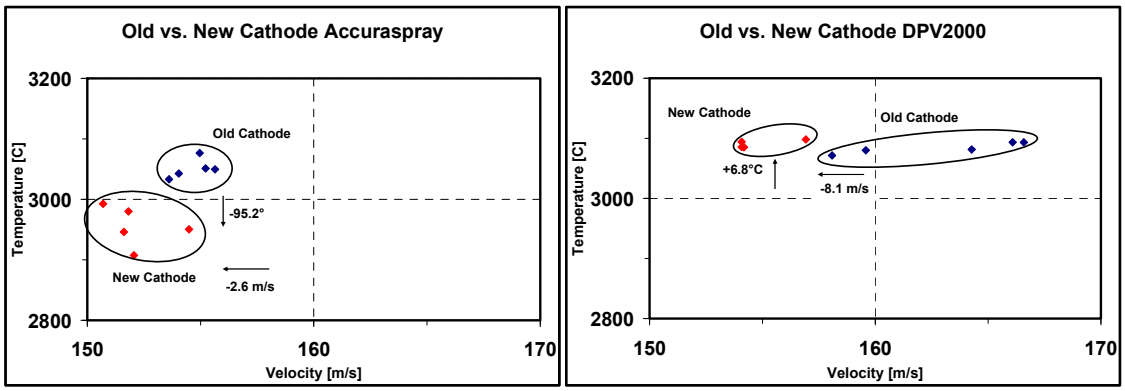

Figure 5.2-2. Average TV from old and new cathode runs measured by Accuraspray (left) and DPV2000 (right).

A deeper look into the individual particle data from the DPV2000 was performed to detect any changes in TV distributions. Figure 5.2-3 shows the truncated TV data measured by DPV2000 for the old and new cathode. It can be seen that the cloud has shifted slightly to the left, indicating a drop in velocity, and the clouds are more tightly overlapped, indicating a reduction in variability. The range of average values decreased from 25.7 C to 14.8 C, and from 8.4 m/s to 3.0 m/s. The range of standard deviation values for temperature also decreased, from 3.12 C to 1.1 C while the velocity standard deviation remained the same.

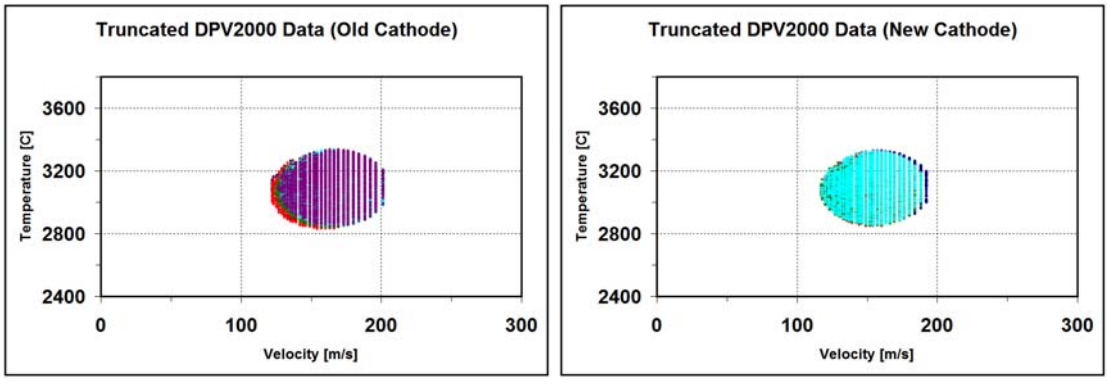

Figure 5.2-3. Truncated DPV2000 data of TV distributions from old (left) and new (right) cathode runs.

Figure 5.2-4 shows the truncated melting index and kinetic energy of the data collected from the DPV2000. The overall average of the melting indexes increased 0.022, and the kinetic energy reduced by 0.52×10^{-7} Joules. This means that there is a greater amount of thermal energy transferred to the particles with the new cathode. The average kinetic energy decreased after replacing the cathode, which is in part a result of the decreased particle velocities.

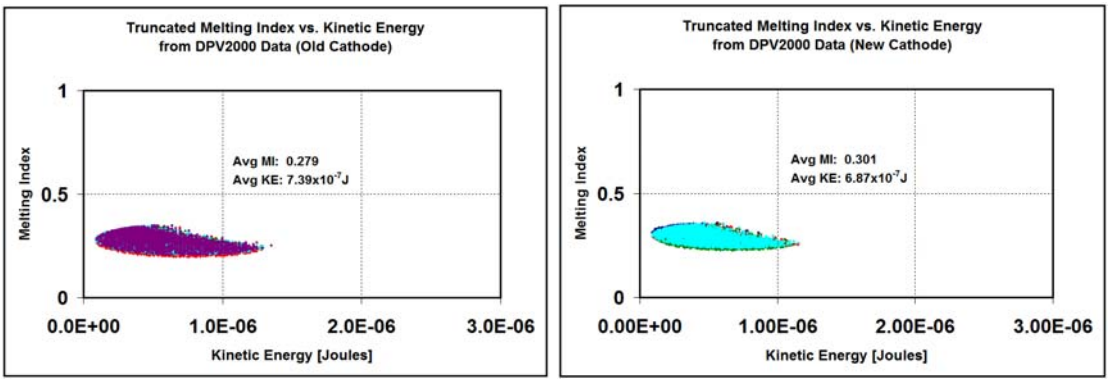

Figure 5.2-4. Truncated melting index and kinetic energy distributions of old (left) and new (right) cathode runs.

Figure 5.2-5 displays the effect of a cathode change on three specific spray conditions measured by Accuraspray; low, medium and high energy. All of the spray condition showed a consistent increase in temperature data. This data was consistent with the previous experiments of the entire process map and repeated center conditions. The effect of a cathode change on coating deposition can also be seen in Figure 5.2-5. All three conditions sprayed show an increase in coating thickness. The average thickness per pass increased about 2 µm, which over thirty passes lead to about a 60 µm difference in coating thickness. This was expected looking at the previous melting index data, since a higher MI typically leads to better deposition efficiency.

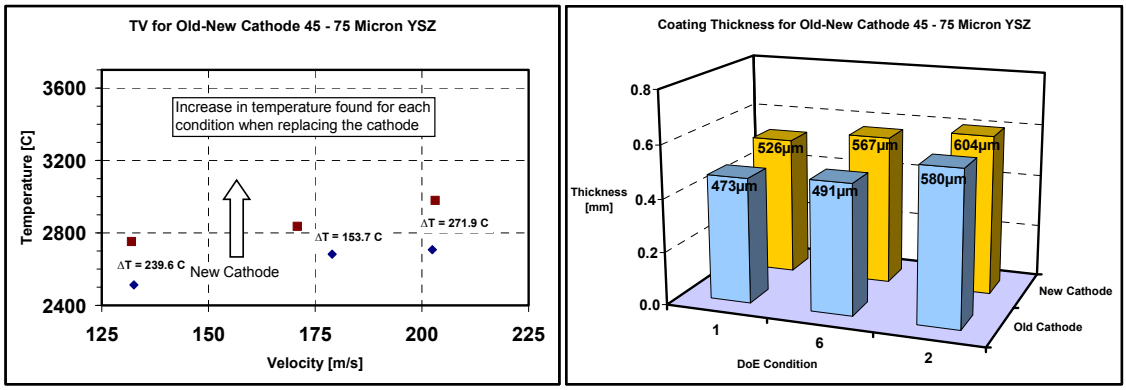

Figure 5.2-5. Effect of cathode change on TV (left) and deposition efficiency (right) for high, medium, and low energy plasma conditions.

5.3 Conclusion: Effect of Hardware Degradation on Particle State and Coating

Changing the cathode of the METCO F4 torch causes a slight change in the measured T&V of in-flight particles. Measuring the TVs for entire process maps before and after changing a cathode shows that the average TVs were within the 2σ standard deviation for most conditions and very close for the remainder. This means that one run after changing the cathode might not have any greater difference than turning off and turning on the spray torch. But, for the tighter conditions the new cathode TV is right at the 2σ limit. For these conditions there might be a significant change in average TV that shifts the distribution and puts some data beyond the 2σ window. When the same center condition is repeated, the cluster of data points has an apparent shift in TV space. The cathode change also had a significant effect on deposition efficiency for the three tested torch conditions (low, medium, and high energy). An average 2 µm per pass increase led to an average 60 µm difference in coating thickness. This is a cause for concern since rate of deposition and coating thickness are directly linked to the coating properties.

6 Variability in Production Environment (Tinker Air Force Base)

Because the thermal spray process is not just limited to only the highly controllable laboratory setting and is widely used in industry, the variability in a real production environment was of interest. In the following experiments, the methods and practices developed at CTSR were applied to an industry spray shop to find out what effects, if any, would occur and if they could be of some benefit. The ambition was to find any anomalies or un-optimized areas in their spray process, especially ones that add to coating variations, and offer solutions to correct them to make a more reliable and predictable coating. The shop was equipped with the F4 plasma torch, using a mixture of argon and hydrogen as plasma and carrier gasses, and YSZ HOSP as the powder material. They were also equipped with the Accuraspray in-flight particle diagnostic sensor. To add value to this exercise, the ICP sensor was brought to this facility and set up in their spray booth to make a series coatings. ICP measurements have never before been performed at this facility and were used to analyze their current coating deposition properties at their typical spray conditions.

6.1 Procedures of Experiments

6.1.1 Design of Experiment

A process map was created around Tinker's primary YSZ spraying condition using the JMP software from SAS (Figure 6.1-1). The process map's TV space was significantly smaller than the map space used in CTSR at Stony Brook due to the 'close to boundary' starting parameters of Tinker. 'Close to boundary' means that the condition was near the limit of safe operating parameters of the particular torch, Sulzer F4. The resulting spray conditions can be seen in the following figure.

Design of Experiments to synthesize a 1st order process map (T-V Diagram)

Condition	Argon [cf/h]	Hydrogen [cf/h]	Current [A]
1	80	21	550
2	68	25	600
3	92	17	600
4	80	21	550
5	68	25	500
6	68	17	600
7	92	25	600
8	80	21	550
9	92	17	500
10	68	17	500
11	92	25	500
12	80	21	550

Each condition has its own unique variability.

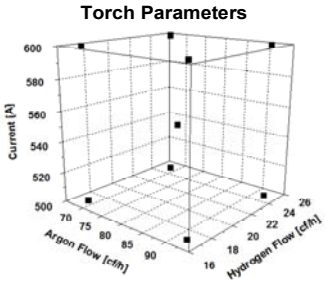

Figure 6.1-1. Design of process map and the torch settings for each condition.

6.1.2 Procedures: Injection Optimization

Particle injection is a very complicated topic that introduces many variables into the plasma spray process [35]. There are a whole array of different injection configurations and techniques. In this experiment the injection is external (radial) which uses a feeding hose attached to metal nozzle tip near the plasma. This allows the operator to choose different injection angles and offset distances from the plasma plume, leading to different particle plume geometry. This translates into different coating properties and microstructure.

Controlling the particle injection is very important when making a repeatable coating. For this experiment, a series of spray runs were performed using the 'in house' method of fixed carrier gas set to a value considered to be 'un-optimized' for this study. In order to optimize the injection, the center axis of the torch needed to be aligned with the optical axis of the Accuraspray's sensor head. This was then considered the reference axis from which to measure plume position. Then the injection optimization experiment was carried out by varying the injection carrier gas incrementally while taking sensor data. Each condition used the same plasma gas flow rates and current input. The optimum carrier gas setting was found by plotting the data in TV space and calculating

the point where maximum temperature and velocity occurred. After the optimum plume position for Tinker's combination of powder-injector-nozzle was found, the same experiment was run a second time in order to confirm the results. This plume position was used for all spray conditions labeled 'optimum'.

To achieve the optimum plume dip for each spray run the spray torch was brought to the Accuraspray sensor and the plume position was monitored while varying the carrier gas until the correct value was achieved. This was performed before each experiment to ensure consistency.

6.1.3 Procedures: Repeated Particle State in Production Environment

Three process maps were made using Tinker's standard practice of holding the carrier gas constant for all conditions (un-optimized injection). Then a new process map was created using the new optimized plume position for each spray condition (one optimized process made due to lack of time). This was done by taking a measurement of plume position at each different combination of torch settings and adjusting the carrier gas accordingly till the optimal plume position was achieved. Each process map was made within a half hour period, back to back with a few minutes break in between. The Accuraspray data was plotted in TV space to visualize the variability of each spray condition and the effects of injection optimization.

6.1.4 Procedures: Coating Repeatability

The ICP sensor was fixed to a stable surface in the spray booth. The sensor was positioned so that the face of the substrate was aligned with the lateral motion of the robot carrying the spray torch. A ladder spray program was created and saved. The program moved the torch horizontally across the substrate at a constant velocity, overshooting each end by five inches, while taking small steps in the vertical direction

after each stroke. The aluminum substrates were the same samples used at CTSR Stony Brook in the previous experiments, 6061-T6 with dimensions of 9”x1”x0.125”. The samples were also prepared in the same way (cleaned and grit blasted) before being loaded into the ICP sensor. Cooling air was consistently applied to the back of the substrate via the ICP sensor’s air jets. The data acquisition software was started and spraying began. Two preheating passes were done before the powder was turned on. After 30 passes were performed, the torch was shut off and the sample was allowed time to cool to room temperature while the ICP collected data. A series of coatings were made on the ICP sensor using both optimized and un-optimized spraying conditions. The substrate temperature and displacement was continuously measured and recorded during spraying. The samples’ weight and thickness were recorded for later analysis.

6.2 Results: Variability in Production Environment

6.2.1 Results: Injection Optimization

The injection optimization experiment results can be seen in Figure 6.2-1. A second order polynomial was used to interpolate the peak of the measured values. The temperature peaks were found with the carrier gas set to 5.5cf/h and 5.9cf/h. Each value of carrier gas had a corresponding measurement of plume position. These two values were averaged and used as optimal plume position.

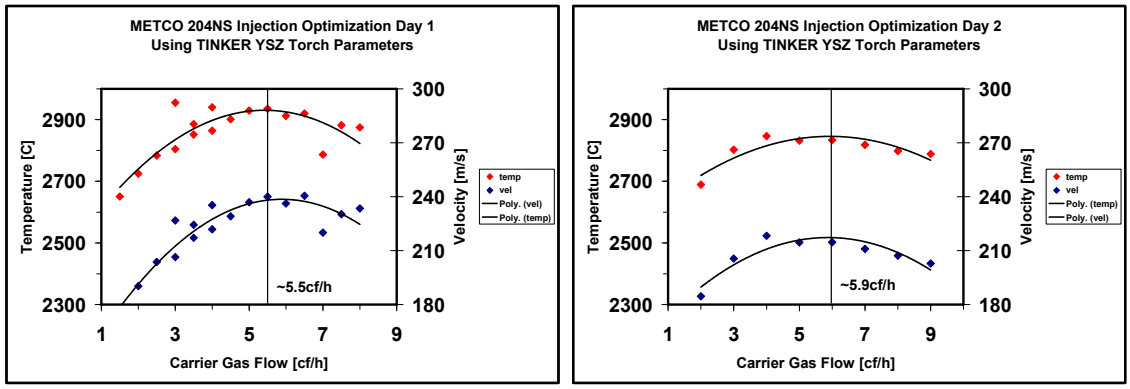

Figure 6.2-1. First (left) and second (right) injection optimization measured by Accuraspray. Both temperature and velocity data are shown.

6.2.2 Results: Repeated 1st Order Map

The series of process maps created at Tinker Air Force Base can be seen in Figure 6.2-2. The three unoptimized process map points are shown scattered in TV space, organized by color to each condition. The optimized points are shown contained within a circle. All of the center condition points (unoptimized and optimized) are shown contained within a large circle to separate from the rest of the map. Although there was only enough time to run one optimized process map, it was observed that the 'optimized' points were consistently hotter and faster. This was expected due to the nature of the injection optimization procedure. Although the injection was optimized for only the center condition, the effect carried through to the others with varied plasma gas flow rates. This demonstrated the importance of plume position rather than carrier gas measurement. The same carrier gas setting was producing different plume positions based on the different plasma gas flow rates. This was undesirable because it lead to different plume penetration.

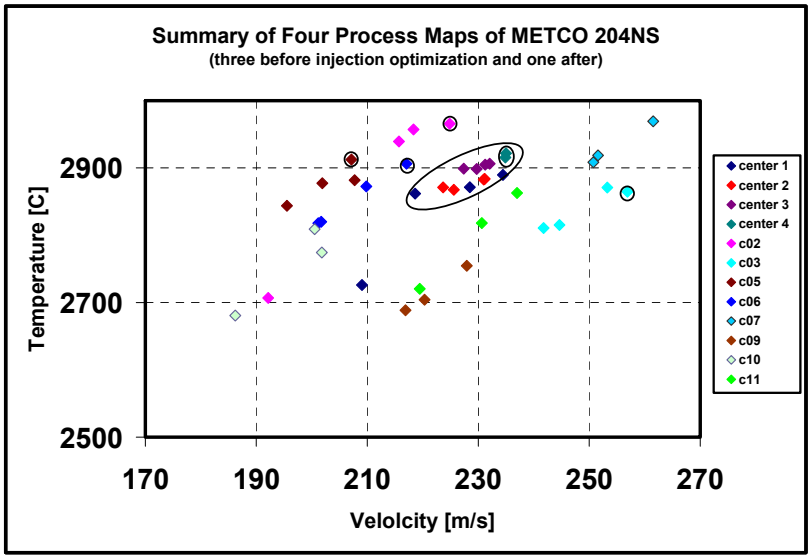

Figure 6.2-2. T&V space showing both un-optimized and optimized process maps.

6.2.3 Results: Coating Repeatability

Following the common practice of CTSR at Stony Brook, measurements of in-flight particle characteristics were taken before making each coating on the ICP sensor. The spray stream's average TV (left) and average MI-KE (right) for each coating is shown below in Figure 6.2-3. The set of unoptimized points is shown as the slower and cooler set of particles with a relatively wide TV distribution. The optimized points show a clear reduction in temperature and velocity variability due primarily to the implementation of injection optimization. There was also an expected increase in both T and V as seen previously in the process maps. The melting index and kinetic energy was calculated using the mean particle diameter and the sensor's average TV measurement. The effect of injection optimization carried over to affect the grouped particle parameters as well, raising the average MI-KE and reducing its variability.

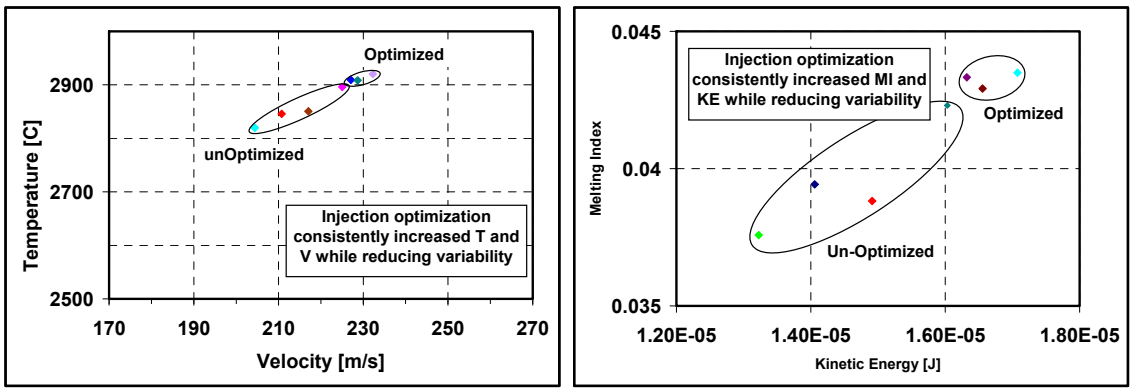

Figure 6.2-3. Effect of injection optimization on the repeatability of DoE center condition used to make ICP samples.

The benefits of injection optimization were further reinforced by the ICP sensor data shown in Figure 6.2-4. The range of final displacements for the optimized cases was greatly reduced, from 0.092mm to 0.018mm (~80%). Because the same substrates and the same spray conditions were used, the results prove that the coating was more consistently deposited. When the ICP data was analyzed using stress calculating software developed at CTSR, a large reduction in coating property variability became

evident (see Table 6.2-1). The greatest reduction was found with the residual stress, with the range of stress dropping from 8.00 MPa to 1.00 MPa (~88%). Also, a large reduction in Elastic Modulus variability was detected, dropping from 5.49 GPa to 0.98 GPa (~82%).

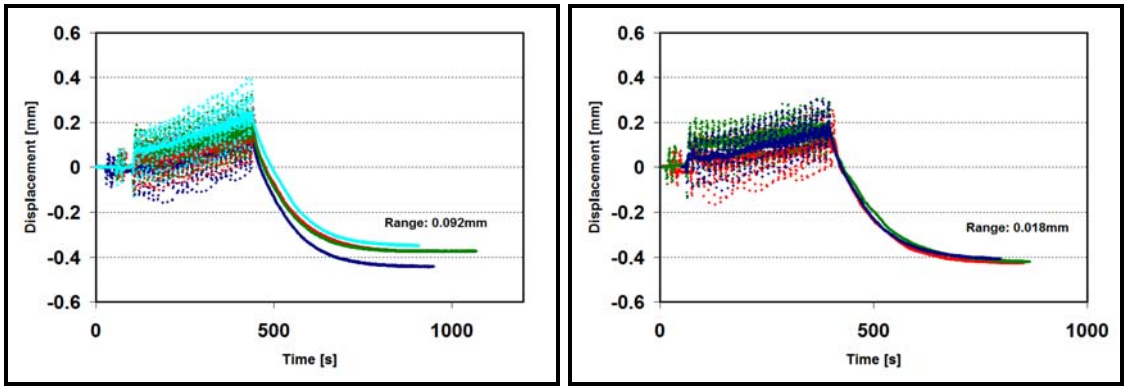

Figure 6.2-4. Un-optimized (left) and optimized (right) heating and cooling displacement curves of ICP sensor samples while spraying.

Unoptimized Coatings				
Sample	**Evolving Stress [Mpa]**	**Thermal Stress [Mpa]**	**Residual Stress [Mpa]**	**Elastic Modulus [Gpa]**
R001	14.60	58.60	-44	19.66
R002	15.25	53.25	-38	21.44
R003	18.96	55.96	-37	21.26
R004	18.56	54.56	-36	25.15
Range	4.36	5.35	8.00	5.49
Optimized Coatings				
Sample	**Evolving Stress [Mpa]**	**Thermal Stress [Mpa]**	**Residual Stress [Mpa]**	**Elastic Modulus [Gpa]**
R005	13.07	52.07	-39	20.00
R006	13.70	53.70	-40	19.21
R007	14.88	54.88	-40	20.19
Range	1.81	2.81	1.00	0.98
% Reducton	58%	47%	88%	82%

Table 6.2-1. Coating properties before (top) and after (bottom) injection optimization, calculated from ICP data using CTSR software.

The final thickness of each sample was also affected by the injection optimization (Figure 6.2-5). The total average thickness increased by about 15 microns (~5%). The higher thickness was a result of an increase in deposition efficiency. There wasn't seen, however, any effect on the thickness variability which remained at 5 microns.

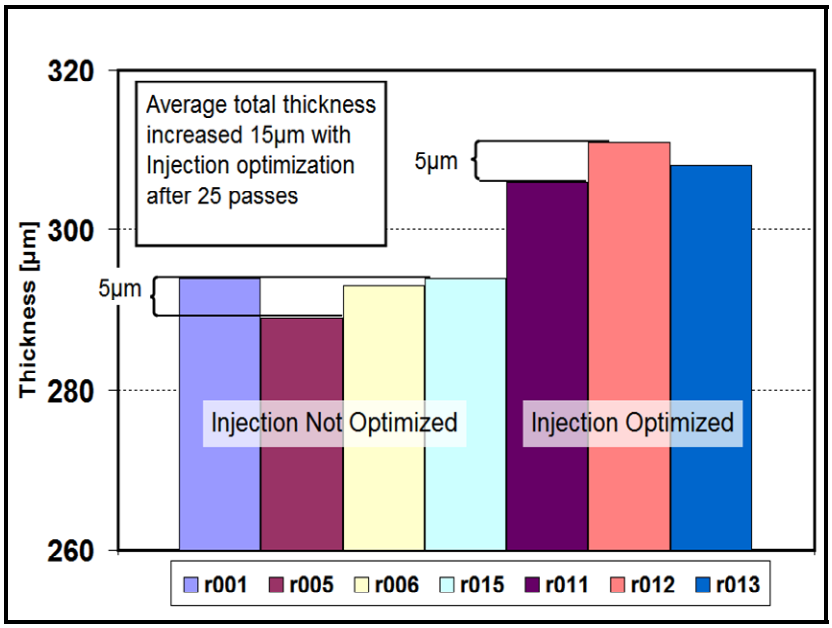

Figure 6.2-5. Coating thickness of samples sprayed on ICP sensor.

6.3 Conclusion: Variability in Production Environment (Tinker Air Force Base)

The injection optimization experiment successfully determined the best plume position that would fully utilize the plasma's energy transfer to the sprayed particles. A clear reduction in TV variability with a raise in average temperature and velocity was shown to be a direct result of the injection optimization. The coatings made after optimizing Tinker's injection had higher deposition efficiency and greater total thicknesses than the conditions used that were considered standard practice. The coatings made on the ICP sensor showed more consistent final deflections after optimization, meaning a more consistently deposited coating. After calculating the coating properties using CTSR's stress analysis software, a large reduction in variability was detected for evolving stress, thermal stress, residual stress, and elastic modulus. The largest reduction in variability was seen for residual stress,

Implementation of injection optimization results in a reduction of wasted material that doesn't adhere to the substrate. This translates into a lot of money saved as this

facility goes through a large amount of spray material per year. Also, more consistent coating properties results in less rejected parts because reducing coating property variability lowers the risk that the coating will not meet spec.

7 Feasibility Study on Feedback Control Using Particle State

The desire to reduce the variability of thermally sprayed coating properties was the impetus behind the following experiments. The following tuning process goes one step further into exploring the extent of controllability of the thermal spray process [36] and how much reduction in variability can be achieved [13]. Details of previous tuning experiments can be seen in [33].

The following tuning experiments make use of regression equations to characterize all the possible outcomes of the spray process. Regression equations are used to describe a set of measured data with respect to a set of input parameters. Regression equations have been used successfully to reproduce in-flight particle properties (temperature and velocity) of a known material after collecting data from a set of "design of experiments" conditions [37]. It was found that once the data was collected from each condition, a regression equation could be created to predict each input parameter's influence on particle state and further more coating properties.

The generic regression equation is shown below in Equation 11. For plasma spraying, the input parameters (primary process parameters) are argon flow rate, hydrogen flow rate, and current. The response parameter is the desired output, such as the particle temperature, particle velocity, coating density, etc. The regression equation is the foundation for the tuning method described in the following section

.

$$R = C_1 + C_2\left(P_1 - \bar{P}_1\right) + C_3\left(P_2 - \bar{P}_2\right) + C_4\left(P_3 - \bar{P}_3\right) + C_5\left[\left(P_1 - \bar{P}_1\right)\left(P_2 - \bar{P}_2\right)\right]$$
$$+C_6\left[\left(P_1 - \bar{P}_1\right)\left(P_3 - \bar{P}_3\right)\right] + C_7\left[\left(P_2 - \bar{P}_2\right)\left(P_3 - \bar{P}_3\right)\right] \quad (11)$$
$$+C_8\left[\left(P_1 - \bar{P}_1\right)\left(P_2 - \bar{P}_2\right)\left(P_3 - \bar{P}_3\right)\right]$$

R: response parameter
C_1: intercept
P_1 to P_3: primary process parameters
$\bar{P}_1$ to $\bar{P}_3$: mean of primary process parameters used to obtain data
C_2 to C_8: parameter effect constants obtained from fit

7.1.1 Feedback Control Using Average T and V

Tuning to achieve repeatable T&V is highly desired because of the inherent drift involved when operating the equipment of different days. Typically, measured in-flight particle data is summarized to an average value for concise reporting. To create the average TV tuning algorithm, a first order TV process map must be created. The process map's average TV values must be used to generate regression constants for four regression equations, two for temperature and two for velocity (in this study the JMP software was used). The response parameters of the four equations are "present temperature", "present velocity", "target temperature", and "target velocity". These equations are used to solve for the three unknown input parameter variables. First the present torch parameters must be input into equations 12 and 13. Then equations 16 and 17 must be applied to "shift" the TV surface described by the regression equation to match the present measured TV values. By fixing one of the input parameters, the other two can be solved. This process can be repeated until the measured TV values converged within an acceptable range of the target TV.

$$T_p = T_1 + T_2\left(A_p - \overline{A}\right) + T_3\left(H_p - \overline{H}\right) + T_4\left(I_p - \overline{I}\right) + T_5\left[\left(A_p - \overline{A}\right)\left(H_p - \overline{H}\right)\right]$$
$$+T_6\left[\left(A_p - \overline{A}\right)\left(I_p - \overline{I}\right)\right] + T_7\left[\left(H_p - \overline{H}\right)\left(I_p - \overline{I}\right)\right] \quad \textbf{12}$$
$$+T_8\left[\left(A_p - \overline{A}\right)\left(H_p - \overline{H}\right)\left(I_p - \overline{I}\right)\right]$$

T_p: present temperature calculated by regression equation
T_1: temperature intercept
T_2 to T_8: calculated parameter effect constants
A_p: present argon flow
$\overline{A}$: mean argon flow from process map
H_p: present hydrogen flow
$\overline{H}$: mean hydrogen flow from process map
I_p: present current
$\overline{I}$: average current from process map

$$V_p = V_1 + V_2\left(A_p - \overline{A}\right) + V_3\left(H_p - \overline{H}\right) + V_4\left(I_p - \overline{I}\right) + V_5\left[\left(A_p - \overline{A}\right)\left(H_p - \overline{H}\right)\right]$$
$$+V_6\left[\left(A_p - \overline{A}\right)\left(I_p - \overline{I}\right)\right] + V_7\left[\left(H_p - \overline{H}\right)\left(I_p - \overline{I}\right)\right] \quad \textbf{13}$$
$$+V_8\left[\left(A_p - \overline{A}\right)\left(H_p - \overline{H}\right)\left(I_p - \overline{I}\right)\right]$$

V_p: present velocity calculated by regression equation
V_1: velocity intercept
V_2 to V_8: calculated parameter effect constants

$$T_t = T_1 + T_2\left(A_t - \overline{A}\right) + T_3\left(H_t - \overline{H}\right) + T_4\left(I_t - \overline{I}\right) + T_5\left[\left(A_t - \overline{A}\right)\left(H_t - \overline{H}\right)\right]$$
$$+T_6\left[\left(A_t - \overline{A}\right)\left(I_t - \overline{I}\right)\right] + T_7\left[\left(H_t - \overline{H}\right)\left(I_t - \overline{I}\right)\right] \quad \textbf{14}$$
$$+T_8\left[\left(A_t - \overline{A}\right)\left(H_t - \overline{H}\right)\left(I_t - \overline{I}\right)\right]$$

T_t: target temperature calculated by regression equation
A_t: target argon flow
H_t: target hydrogen flow
I_t: target current

$$V_t = V_1 + V_2\left(A_t - \bar{A}\right) + V_3\left(H_t - \bar{H}\right) + V_4\left(I_t - \bar{I}\right) + V_5\left[\left(A_t - \bar{A}\right)\left(H_t - \bar{H}\right)\right] + V_6\left[\left(A_t - \bar{A}\right)\left(I_t - \bar{I}\right)\right] + V_7\left[\left(H_t - \bar{H}\right)\left(I_t - \bar{I}\right)\right] + V_8\left[\left(A_t - \bar{A}\right)\left(H_t - \bar{H}\right)\left(I_t - \bar{I}\right)\right] \quad \textbf{15}$$

V_t: target velocity calculated by regression equation

$$T_{\text{target}} - T_{\text{present}} = T_{\text{t}} - T_{\text{p}} \quad \textbf{16}$$

T_{target}: target temperature
T_{present}: present temperature measured by sensor

$$V_{\text{target}} - V_{\text{present}} = V_{\text{t}} - V_{\text{p}} \quad \textbf{17}$$

V_{target}: target velocity
V_{present}: present velocity measured by sensor

7.2 Procedures: Feasibility Study on Feedback Control Using Particle State

7.2.1 Experiment 1: Feedback Control Using Average T and V

The goal of this experiment was to use the average TV tuning method to achieve a desired average particle TV within a window of ±2 m/s and ±15 C. This was done by first creating a first order process map using the 12 DoE conditions. The powder feeder was set feed at a rate of 2 g/m. Using the JMP software, regression equations were generated for temperature and velocity. The 'primary process parameters' of the equations were argon flow rate, hydrogen flow rate, and current. A target temperature and velocity were chosen and regression equations were used to produce starting torch parameters. The next step was to operate the torch and measure the present T and V to use as inputs into the regression equations. The equations were used to calculate the distance between the present particle state and the desired particle state. A new set of

torch parameters were generated and the process was repeated until the T&V were within the acceptable window.

7.2.2 Experiment 2: Feedback Control Using Average T and V to Produce Coatings

This experiment went one step past achieving only a repeatable TV. A series of coatings were made at the conditions where the in-flight particle measurements were within the acceptable window of TV, 20 C and 2 m/s. This "tight" window was designed to cover a smaller area of TV space than the measurements resulting from previous experiments repeating the same conditions. This experiment tested the variability of coating properties as a function of in-flight particle characteristic variability.

The first set of torch input parameters starting point were generated using the tuning algorithm. The powder feeder calibrated to feed 2.0 g/m. The torch was ignited and the first set of diagnostic measurements was taken using the DPV2000. This data was quickly analyzed to determine the average TV measured. If these values were outside the predetermined acceptable TV window, the tuning algorithm was run iteratively until acceptable values were achieved. At this point, the ICP's data acquisition software was started. The coating was made by first preheating the sample with two ladder routine passes. The ICP cooling air was set to 40 psi and opened to cool the backside of the substrate. The powder feed rate was then turned up to 30 g/m and the robot's ladder spray program was initiated, running a total of 30 coating passes. When finished, the coating was allowed time to cool to room temperature.

The in-flight particle data collected was used to generate a series of histograms to compare one spray run to another. The bi-modal curve fitting algorithm was used to calculate the defining characteristics of each histogram (averages and standard deviations of the two peaks and the scaling factor).

7.3 Results and Discussion: Feasibility Study on Feedback Control Using Particle State

7.3.1 Experiment 1: Average TV Tuning

Experiment 1 demonstrates how a reduction in TV variability was achieved by following the aforementioned average TV tuning process. Figure 7.3-1 shows the results of tuning experiment 1 using YSZ HOSP 1. Each iteration of the tuning process brought the average TV closer to the target window. The third and final iteration's results were within the desired TV range. The target overshoot was contributed to the time difference between the date that the process map used to generate the regression equations was created and the actual experiment. In reality, the shape of the process map changes as the hours on the plasma torch accumulate and the parts wear. This was not accounted for when the regression equations were created.

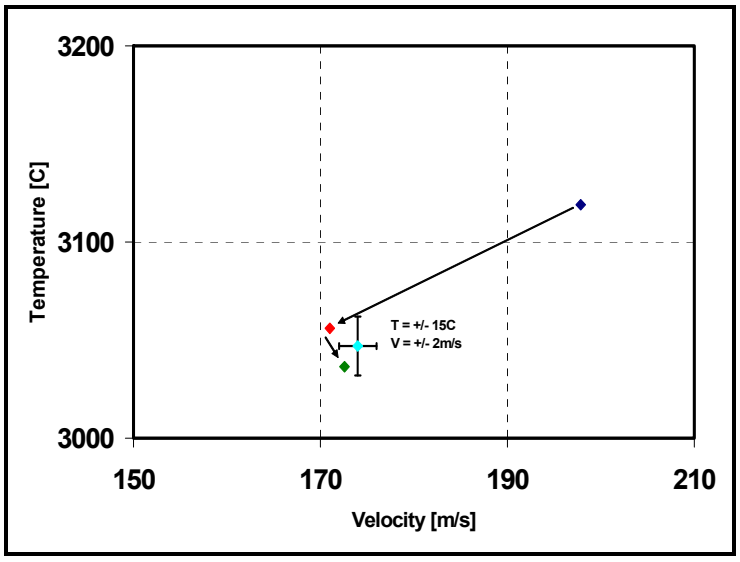

Figure 7.3-1. Tuning Experiment 1: TV data from tuning experiment measured by DPV2000.

The individual in-flight particle data was used to create distribution plots of TV and MI-KE, shown in Figure 7.3-2. The data in the plots is what remained after a 10-90 percent elliptical truncation was performed. From the first to last condition, there was a

clear shift in position and shape of the data point cloud. A clear reduction was noticed in overall MI-KE spread, meaning that more particles were consistently melted.

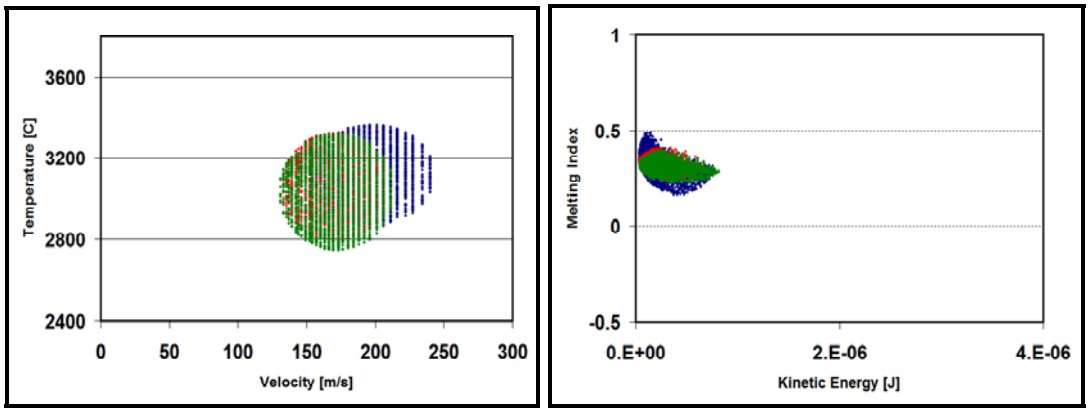

Figure 7.3-2. Tuning Experiment 1: Truncated TV (left) and MI-KE (right) plots made using 5,000 measured particles of DPV2000 data.

A set of histograms were created for temperature and melting index, shown in Figure 7.3-3. The first condition's distributions are shown on the bottom. As the average particle temperature decreased with each iteration, the first peak of the bi-modal histogram was seen to increase. This was a result of more particles sustaining their melting temperature while going through a phase transformation. The melting index histograms mirror this trend due primarily to its dependency on temperature, although particle size also plays a significant role.

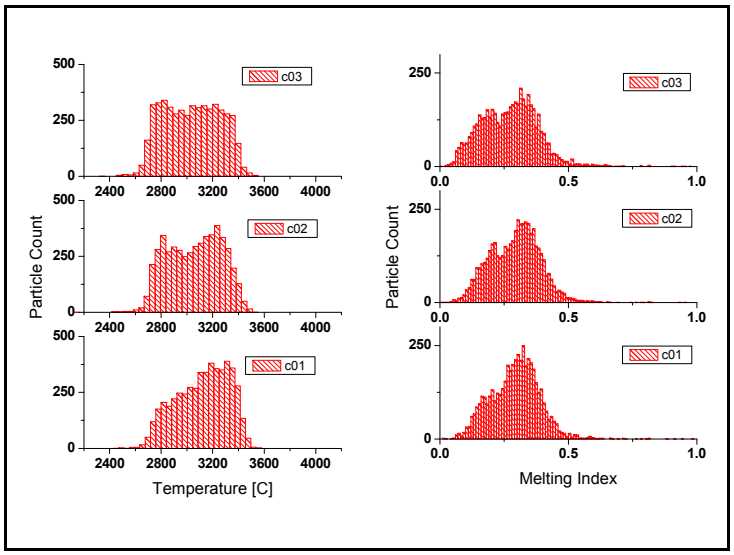

Figure 7.3-3. Tuning Experiment 1: Temperature and melting index distributions.

7.3.2 Experiment 2: TV tuning to produce coatings

This experiment used the average TV tuning process to produce coatings of YSZ HOSP2 on 6061-T6 aluminum substrates while using the ICP sensor to record substrate deflection and temperature. The average TVs measured on the tuning process' final iteration is shown in Figure 7.3-4. All points were within the acceptable window of ±20C and ±2m/s (1% deviation from the target) except for one that has a slightly slower velocity (~6 m/s). The grouped parameters, melting index and kinetic energy calculated from the final tuning iteration are also shown below in Figure 7.3-4. The variability of these parameters was found to be much larger, 11% for melting index and 45% for kinetic energy.

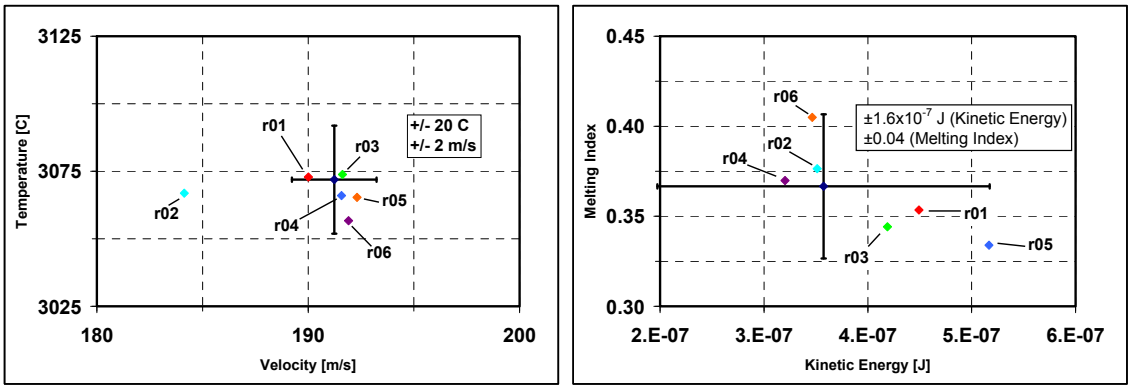

Figure 7.3-4. Final tuned average TV for each coating (left) measured by DPV2000. Average melting index and kinetic energy for each final condition (right).

A total of six runs were carried out, three of which did not need to be tuned. The in-flight diagnostics of these runs taken immediately after turning on the spray torch resulted in a TV measurement that was within the acceptable range. The tuning history of the other three runs can be seen in Figure 7.3-5.

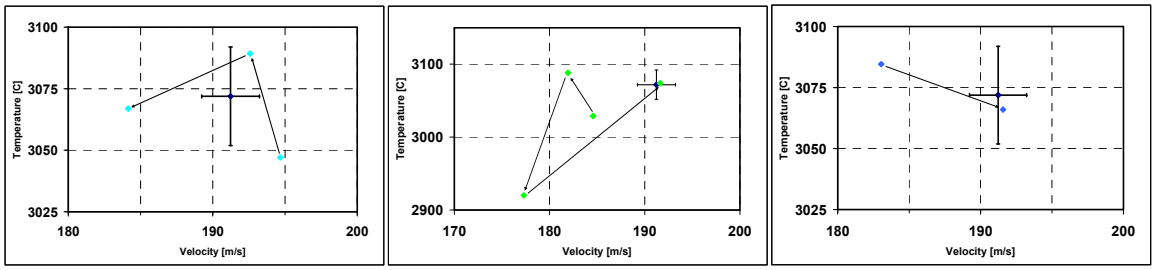

Figure 7.3-5. Iterative process of tuning using temperature and velocity feedback for runs r02 (left), r03 (center), and r04 (right).

The in-flight particle distributions of temperature, velocity, melting index, and kinetic energy were calculated using the data collected by the DPV2000 and can be seen in Figure 7.3-6. To precisely measure the variability of these distributions, the bi-modal curve fitting algorithm was implemented to calculate the distribution characteristics. The curve fitting values are listed in Table 7.3-1. An interesting observation was the high variability present in the kinetic energy distribution characteristics, as high as 57%. One possible explanation for this is the resolution of DPV's velocity measurement capability, which at the average 190 m/s has a gap of 6m/s.

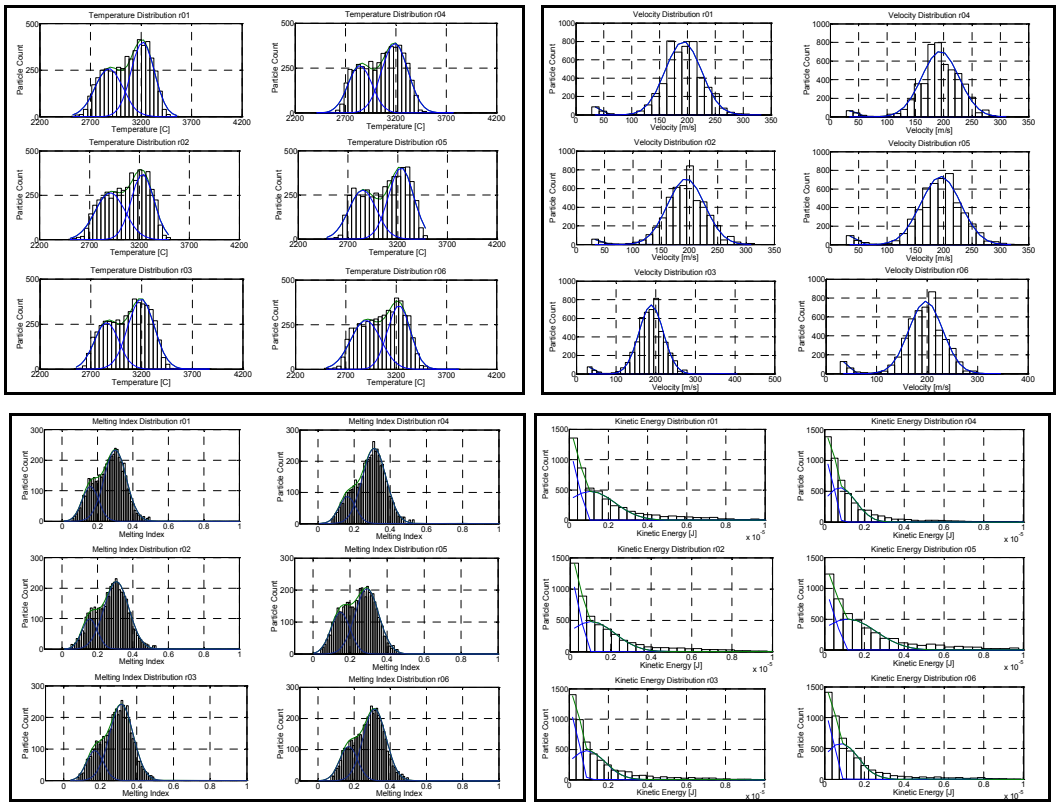

Figure 7.3-6. Temperature, velocity, melting index, and kineti energy distributions with bi-modal curve fitting for final iteration coating condition.

Run	Temperature Distributions					Velocity Distributions				
	mean1	std1	mean2	std2	scaling	mean1	std1	mean2	std2	scaling
r01	2884	138	3218	115	0.43	35	11	193	32	0.04
r02	2856	120	3197	131	0.38	31	15	188	31	0.04
r03	2907	150	3232	114	0.49	29	15	194	33	0.04
r04	2844	118	3190	130	0.38	35	12	194	33	0.03
r05	2848	139	3235	126	0.43	35	12	195	35	0.04
r06	2899	150	3229	114	0.50	36	10	198	33	0.05
Range	63	33	45	17	0.13	7	5	9	4	0.02
Range %	2	24	1	14	29	22	40	5	13	39
Standard Deviation	27	14	19	8	0.05	3	2	3	1	0.01
	Melting Index Distributions					Kinetic Enery Distributions				
	mean1	std1	mean2	std2	scaling	mean1	std1	mean2	std2	scaling
r01	0.16	0.05	0.30	0.06	0.26	3.38E-07	2.02E-07	1.08E-06	1.26E-06	0.28
r02	0.17	0.05	0.31	0.06	0.22	2.51E-07	2.51E-07	9.13E-07	9.32E-07	0.38
r03	0.16	0.04	0.31	0.07	0.22	3.21E-07	1.98E-07	1.03E-06	1.18E-06	0.30
r04	0.16	0.05	0.31	0.07	0.20	2.42E-07	2.26E-07	7.61E-07	7.95E-07	0.33
r05	0.15	0.05	0.29	0.06	0.34	3.70E-07	2.27E-07	1.17E-06	1.40E-06	0.24
r06	0.17	0.05	0.31	0.06	0.27	2.87E-07	2.03E-07	8.11E-07	8.76E-07	0.30
Range	0.02	0.01	0.02	0.01	0.14	1.28E-07	5.29E-08	4.08E-07	6.07E-07	0.13
Range %	14	17	8	12	54	43	24	43	57	44
Standard Deviation	0.01	0.00	0.01	0.00	0.05	5.05E-08	2.05E-08	1.59E-07	2.41E-07	0.05

Table 7.3-1. Bi-modal curve fitting characteristics for each coating's data distribution showing means, standard deviations, and scaling factors.

The raw ICP sensor data can be seen in Figure 7.3-7. Each data point represents the displacement of the substrate at a given time. The first curve sections resembled saw tooth patterns, which resulted from the robot's cyclic path overshooting the substrate on each side before making the next pass. The next curve section occurs after the coating passes were completed and the coating was allowed to cool to room temperature. Immediately after the coating passes finish there was a large change in displacement, followed by an asymptotic approach to the final values. The driving force behind this phenomenon is the thermal mismatch of coating and substrate. The displacement cooling curve closely resembled the temperature cooling curve, rapidly decreasing temperature at first because of higher convection rates and then leveling off as the substrate temperature neared the ambient temperature.

Utilization of the ICP sensor data was essential to calculate the stress state and modulus of each coating. The calculated evolving stresses, residual stress, and elastic modulus for each coating is shown in Table 7.3-2. An interesting fact to point out is that even though the average temperature and velocity variability is very small, the coating property variability is not. Average temperature and velocity variability was only ~1% from the target while the coating property variability was at least ~16% and at most ~122%.

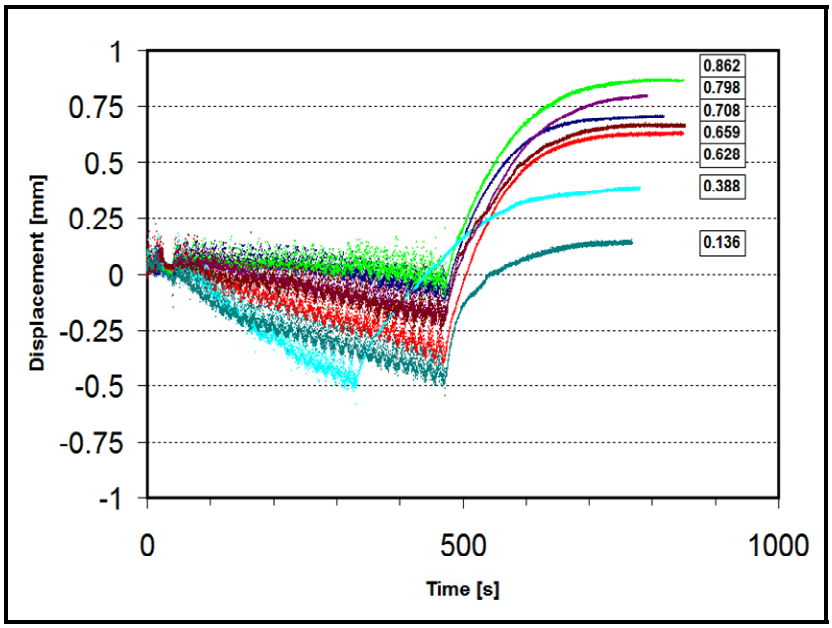

Figure 7.3-7. Tuning Experiment 2: ICP data taken while spraying seven coatings of YSZ HOSP 2 using the tuning process to attain the same TV within +/- 20°C and +/- 2m/s.

Run #	Thickness [µm]	Evolving Stress [Mpa]	Residual Stress [Mpa]	Coating Modulus [Gpa]
r01	535	14.0	-40.9	17.2
r02	617	15.9	-31.0	21.4
r03	589	14.5	-47.4	39.8
r04	546	13.8	-41.2	57.6
r05	608	13.5	-31.0	29.2
r06	672	14.9	-28.4	33.0
Range	137	2.4	19.0	40.4
Percent Range	23	16.6	51.8	122.3
Standard Deviation	50	0.9	7.6	14.5

Table 7.3-2. Coating properties calculated using ICP sensor data from the six tuned spray runs.

7.4 Conclusion: Feasibility Study on Feedback Control Using Particle State

After collecting the data from a series of process map runs, the JMP IN 7 statistical software was used to generate regression equations to describe the TV space with respect to argon flow rate, hydrogen flow rate, and current. It was found that each different run gave slightly different coefficients and therefore different shaped contours. This was understandable because wear on the gun and small changes in operating environment is known to cause in-flight particle states to vary. Because of this, the result

of adjusting one parameter cannot be precisely determined on different days, but a sufficient estimation for tuning purposes can be achieved.

Although the variability in average TV was very small (~1%) the average grouped parameters, TV and MI-KE distributions, and coating properties showed significantly higher values. This encouraged the thought of tuning the thermal spray process using grouped parameters since they more accurately describe each unique particle state with respect to its physical properties.

Tuning the plasma torch to achieve desired in-flight particle properties is believed to be a critical step to make coatings with consistent physical and mechanical properties. While this experiment used a target of average TV, a similar experiment could be created that would tune according to average MI-KE, or some other property from second-order process maps. When a successful tuning method has been discovered, the iterative process of tuning could be applied to a control system that will continuously monitor in-flight particle properties and adjust torch settings.

8 Conclusions

Stability and consistency are critical qualities the thermal spray process must possess so that predictable, reliable, and repeatable coatings can be made. The development of methodical procedures that eliminate the influence of external factors and reduce the process to one that is isolated and controllable is imperative. The accuracy and precision of thermal spray equipment have been tested repeatedly and room for improvement has been revealed, both in the hardware itself and its utilization. The hardware being referred to is the plasma torch controller and diagnostic sensors. Hardware limitations include gas flow controller precision, power controller precision, powder injector type and location, powder feeder consistency, sensor resolution, and sensor versatility. Proper utilization of the available equipment means not only following a set of methodical procedures to reduce random influences on the spray process. It means developing a sound and detailed understanding of equipments operation principles.

The vast number of equipment interactions increases the potential for the process to "drift". This can occur without detection as some parameters cannot be actively monitored. Frequent inspections and maintenance are required to keep the equipment in a known state of operation.

The reliable and consistent operation of diagnostic equipment is a critical factor when comprehensive analyses are performed using their data to predict coating performance. Slight variations in diagnostic measurements propagate themselves through the analysis contributing to error is what is believed to be strong scientific correlation. The use of this equipment is not simple by any means, requiring the input of a plethora of configuration settings that are unique to each spray material and torch configuration. Caution must be taken to ensure comparability between experiments.

The experiments in this thesis have revealed areas of thermal spraying where variability is present and to what magnitude. The experiments contained herein provided examples of practices that should be adopted by any thermal spraying company desiring to improve the efficiency of their spray process. The process control methods discussed in this paper present new techniques that reduce the variability in several aspects of the thermal spray process. They improve confidence in achieving a desired coating, and are applicable to any combination of material and spray condition.

There are a number of different ways in which to interpret and utilize the diagnostic sensor data. Ensemble sensors report single values that result from an average measurement of plume characteristics. They can quickly measure the spray plume's geometry and intensity to give the operator an instant response about how the process is behaving. These sensors are especially useful when there is a high feed rate of particles that makes individual particle detection impossible. In this study, an ensemble sensor was used measure the plume position after injection optimization. For further experiments that utilized injection optimization, the plume position was measured and adjusted using the ensemble sensor to match the optimized value. Sensors that measure individual particles enable a deeper insight into the spray process because individual particle properties can be calculated from the measured data. These particle properties earned the title "grouped parameters" because they encompass a series of thermal and physical characteristics that are unique to each individual particle and powder material.

The average TV tuning experiment in this study demonstrated the limit of controllability that occurs when using only average temperature and average velocity as feedback parameters. While average TV variability was controlled to within 1%, the variability of grouped parameters and coating properties was significantly large. Future experiments will focus on utilizing grouped parameters for tuning feedback in hope to achieve a more consistent melting state and momentum transfer. Experiments featuring distribution based feedback control are also being considered for future work because it is believed that the average property values aren't sufficient descriptors of the spray plume. It has been shown in this thesis that several spray runs where the average in-flight property values varied by only one percent, the individual in-flight particle property distributions varied significantly. The ability to characterize the bi-modal distributions was an essential step for the development of a distribution tuning algorithm. Entire process map distributions were consistently analyzed to develop relationships between spray parameters and distribution characteristics.

Regression analysis enabled the use of empirical data from previously sprayed coatings to produce a mathematical model linking spray parameters to desired outcomes. The work in this thesis focused on in-flight particle properties but this technique could be extended to predict coating properties. This takes thermal spray one step past using "process maps" that simply point the operator in the right direction to the development of an intelligent feedback control system where the spray parameters are chosen and adjusted continuously on a spray to spray basis.

With the knowledge gained through experimentation and detailed exploration of the thermal spray process, the goal of creating a primary reliant coating will be achieved. This will mark a new milestone where thermal spray coatings will be accounted for in the engine design process and will be relied upon to perform without a doubt of failure.

9 Future Work: Feedback Control Using Full Distributions of Particle States

It has been previously stated that the simplified average particle TV does not fully describe the particles molten state or alone accurately predict how it will act upon substrate impact. Previous experiments in this paper have shown that small changes in average TV significantly change the distributions of individual temperature measurements. This usually occurs in the close proximity to the particle's melting temperature where particles have a tendency to get 'trapped' in a phase transformation. There can be an accumulation of particles here that skew distribution characteristics. Although this can be avoided at higher operating temperature where the bi-modal distribution characteristic vanishes, typical plasma operating conditions lie in this critical region.

This section presents a natural extension of the feedback control method using average TV, described in the previous section. Although there have been some advances in this experiment, due to time constraints it is not yet completed. The method of feedback control, discussed in this section, uses the same principle as the aforementioned method of average TV control with the exception that it incorporates the full range of individual in-flight particle data rather than a simplified single number. There are more response parameters and more regression equations to account for the number of distribution characteristics. Distribution feedback control incorporates the concept of bi-modal curve fitting, making the five curve-fit parameters into the five response parameters for the regression equations. The first two response parameters are the average and standard deviation of the first distribution peak, a_1 and σ_1. The second two response parameters are the average and standard deviation of the second distribution peak, a_2 and σ_2. The fifth response parameter is the scaling factor, s, which distributes the data between the two peaks. When an entire process space has been mapped, the user of this algorithm is able to generate a set of input values for the plasma torch by selecting the distribution characteristics that are desired (i.e. a very large number of particles above the melting temperature with a narrow temperature distribution). The equations are solved with the aid of MATLAB or Mathematica software.

9.1 Procedures: Feedback Control Using Full Distributions of Particle States

To achieve a successful distribution tune, a set of histograms for each of the 9 DoE spray conditions must first be created. For this experiment, the goal was to use temperature as the feedback parameter so the histograms were made using the temperature measurement data. The bi-modal curve fitting algorithm was used to calculate the five characteristic parameters for each distribution. A total of 45 parameters were used to generate a set of five regression equations. Each regression equation had one of the five bi-modal characteristic parameters as its response parameter, and the three torch input parameters as its primary process parameters. These equations were solved to produce the first set of torch input values (argon flow rate, hydrogen flow rate, and current). From this point on began the iterative tuning process of setting the torch parameters, measuring in-flight particle characteristics, testing the measured value against the acceptable values, and re-running the algorithm if necessary.

9.2 Results and Discussion: Feedback Control Using Full Distributions of Particle States

The collected in-flight particle data was arranged into histogram representation, shown in Figure 9.2-1. Distinct features can be seen for each of the DoE conditions. Overlaid onto each histogram are the bi-modal curve fits. Table 9.2-1 shows the respective curve fitting characteristics for each bi-modal distribution.

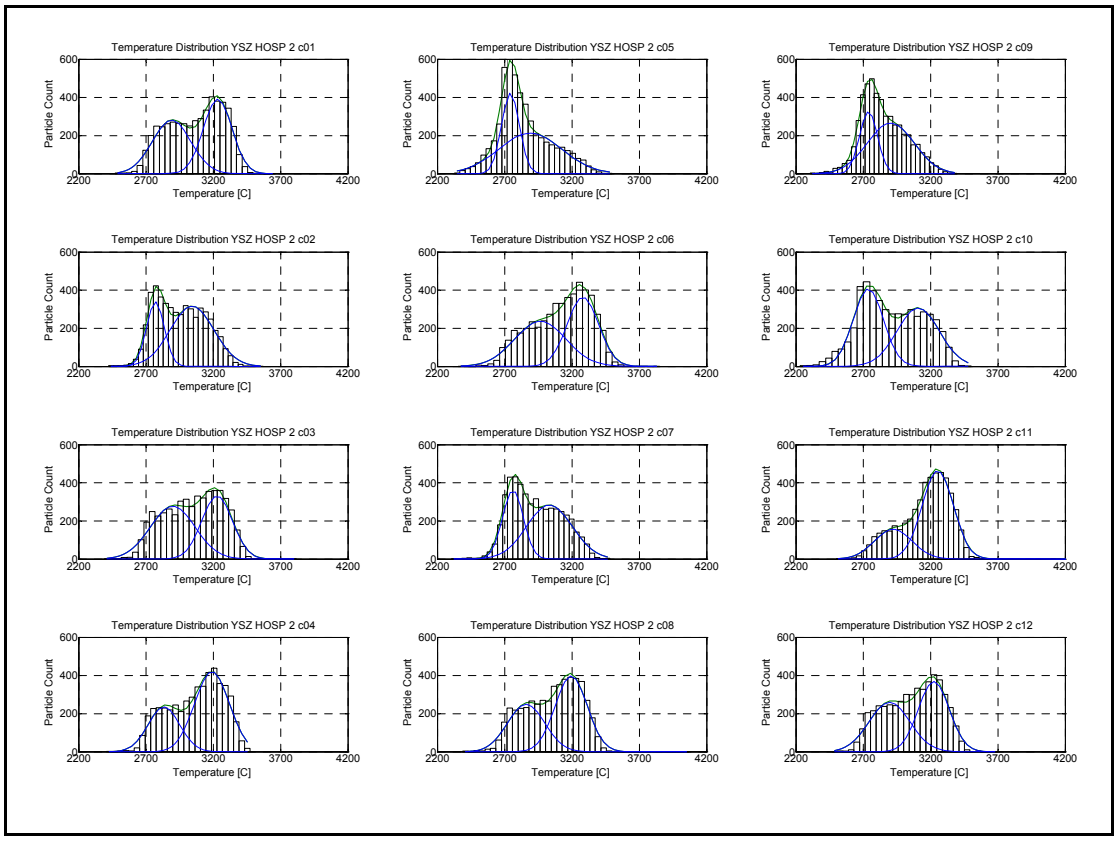

Figure 9.2-1. YSZ HOSP 2 process map temperature distributions showing the result of curve fitting as a sum of two normal distributions.

Condition	Curve 1		Curve 2		Scaling Factor
	Average [C]	Standard Deviation [C]	Average [C]	Standard Deviation [C]	
1	2891	143	3233	106	0.49
2	2770	66	3042	163	0.30
3	2899	166	3229	114	0.55
4	2834	118	3190	129	0.34
5	2743	66	2890	233	0.36
6	2965	190	3280	117	0.51
7	2761	77	3032	169	0.37
8	2860	138	3194	119	0.42
9	2739	67	2904	173	0.32
10	2738	112	3108	157	0.49
11	2923	139	3252	116	0.29
12	2895	152	3224	115	0.48

Table 9.2-1. Details of YSZ HOSP 2 temperature distribution curve fitting. Scaling factor is the ratio of particles distributed to Curve 1.

10 Appendix

10.1 List of Equipment

Equipment	Manufacturer	Model	Serial #
Plasma Torch	Plasma-Technik AG Switzerland	F4	
Plasma Controller	Plasma-Technik AG Switzerland	A3000 S	
Plasma Power Supply	Plasma-Technik AG Switzerland	PT800	
Powder Feeder	Plasma-Technik AG Switzerland	Twin System 10-2	
Robot	Staubli	RX90	
Accuraspray Computer	Technar	g-3	62
Accuraspray Sensor Head	Technar	H / high emission	63
DPV-2000 Controller	Technar	Millennium Edition Software Version 4.0.12	
DPV-2000 XY Scanning Unit	Technar		

Table 10.1-1. Equipment used in this study.

10.2 Reliability of Process Maps: YSZ HOSP 2 Results

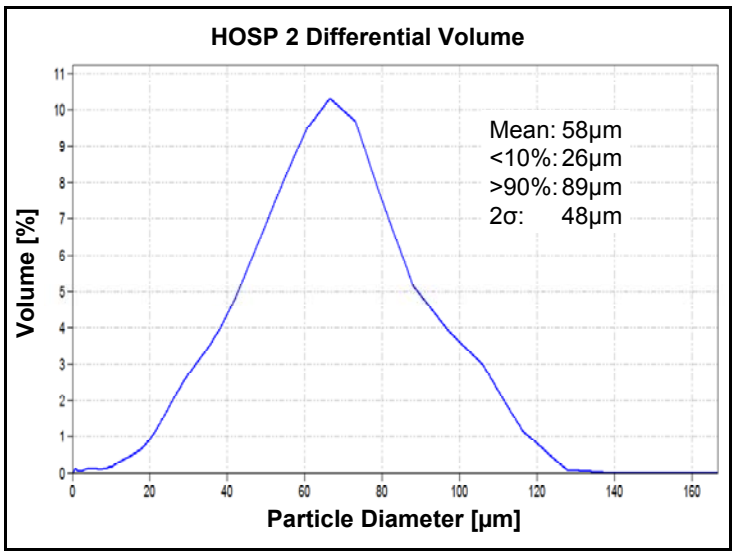

Figure 10.2-1. Particle size distribution of YSZ HOSP 2 powder measured by the Beckman Coulter LS 13 320 Particle Size Analyzer.

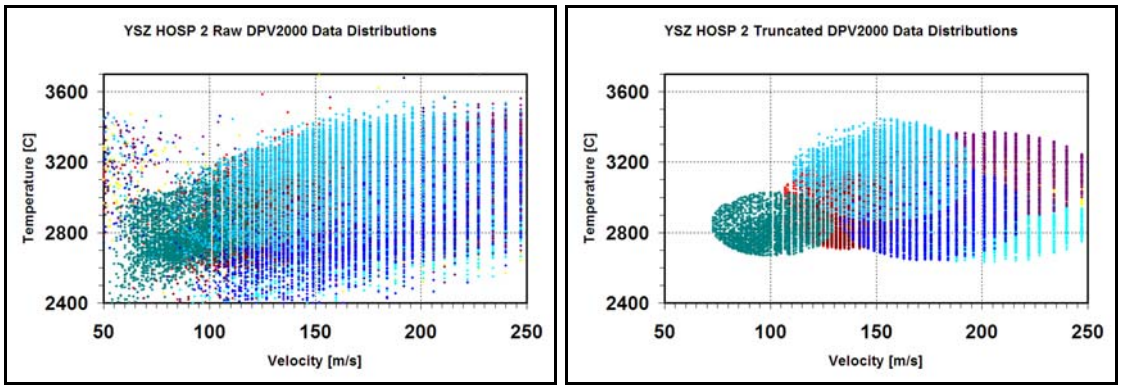

Figure 10.2-2. Temperature-velocity plots of entire YSZ HOSP 2 process map before (left) and after (right) elliptical truncation. Data taken from DPV2000.

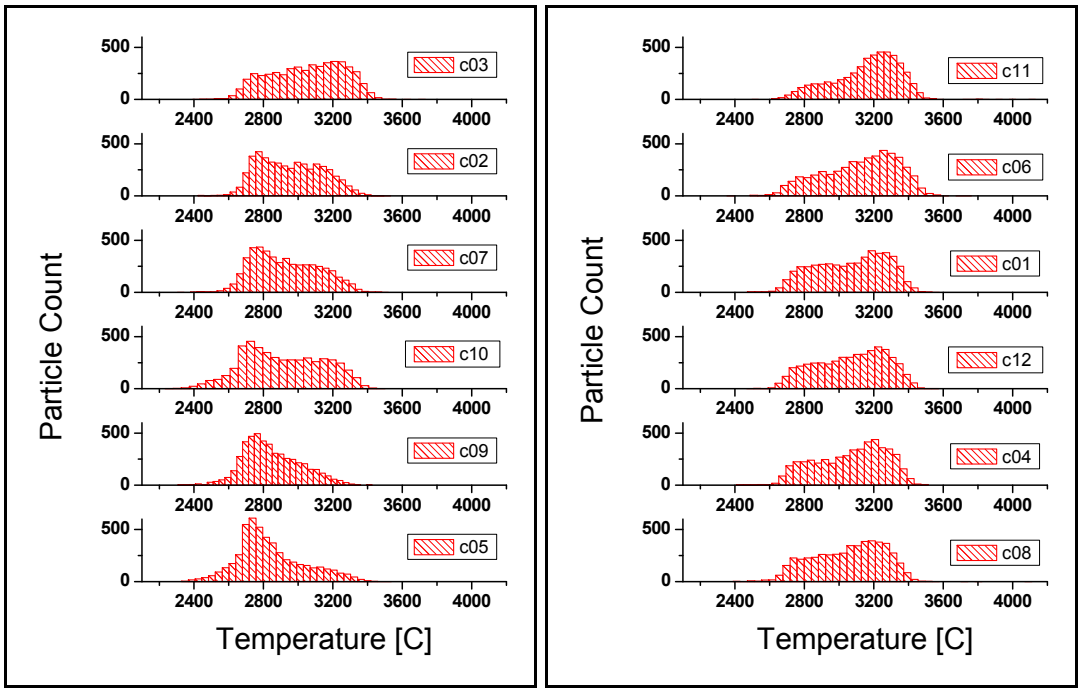

Figure 10.2-3. Temperature distributions for each condition of YSZ HOSP 2 process map. Scott's formula was used for bin sizing.

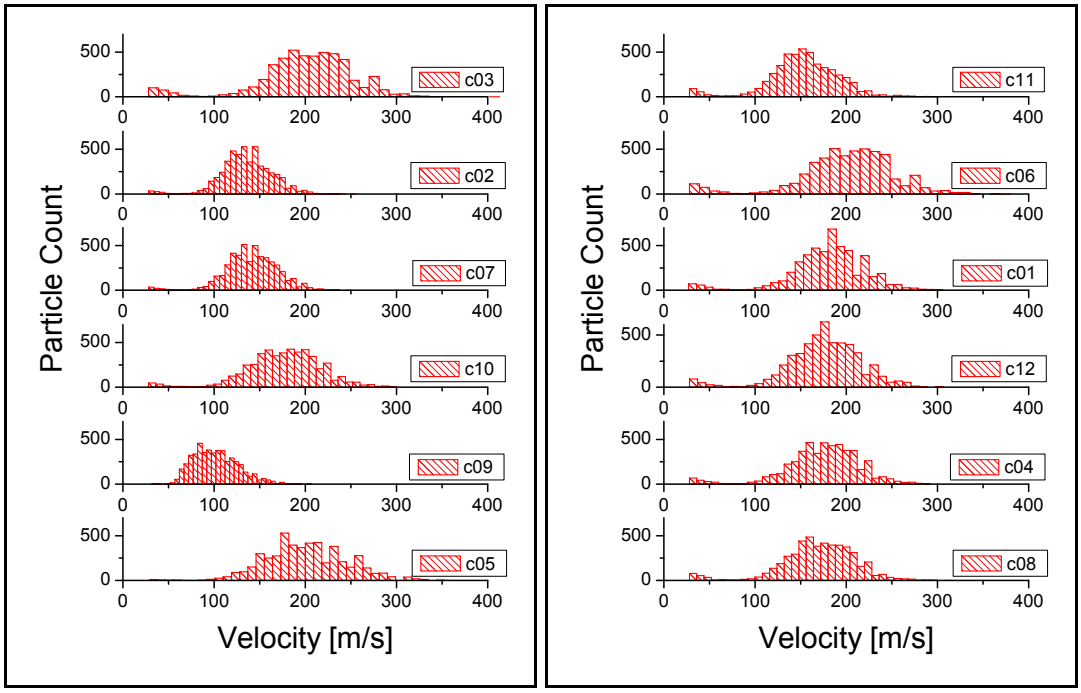

Figure 10.2-4. Velocity distributions for each condition of YSZ HOSP 2 process map. Scott's formula was used for bin sizing.

Condition	T Average [C]	T Standard Deviation [C]	V Average [m/s]	V Standard Deviation [m/s]
1	3066	203	179	43
2	2955	181	135	28
3	3049	208	200	52
4	3066	200	173	42
5	2839	193	201	44
6	3119	214	200	54
7	2928	187	140	29
8	3053	201	169	41
9	2848	165	101	24
10	2912	229	176	41
11	3157	189	153	39
12	3067	202	175	42

Figure 10.2-5. Average T and V values with their standard deviations for YSZ HOSP 2 calculated from DPV 2000 data.

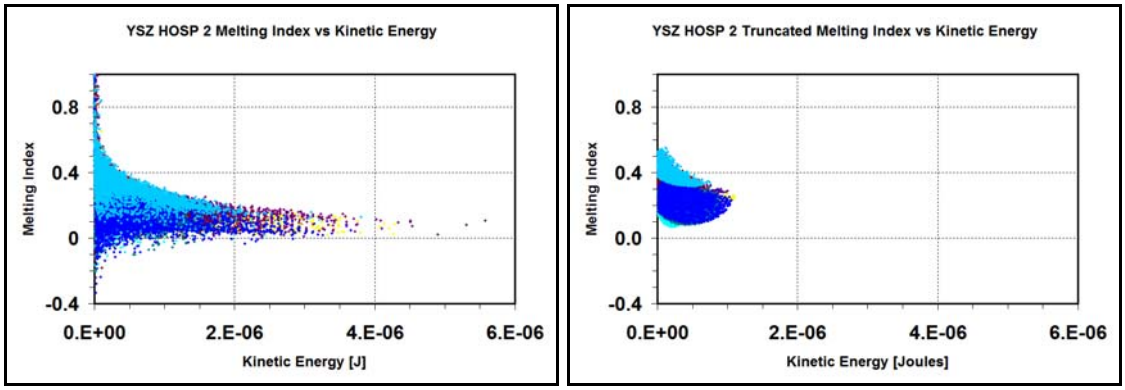

Figure 10.2-6. YSZ HOSP 2 MI-KE plots created plots of raw data (left) and truncated data (right) calculated from DPV2000 data.

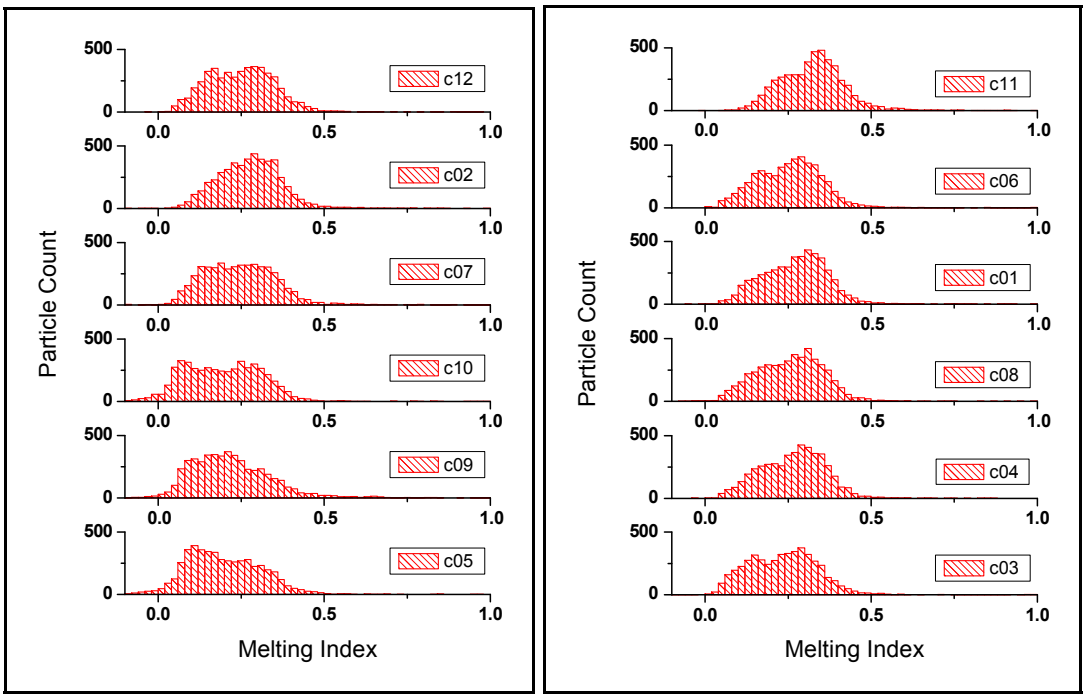

Figure 10.2-7. MI distributions for each condition of YSZ HOSP 2 process map.

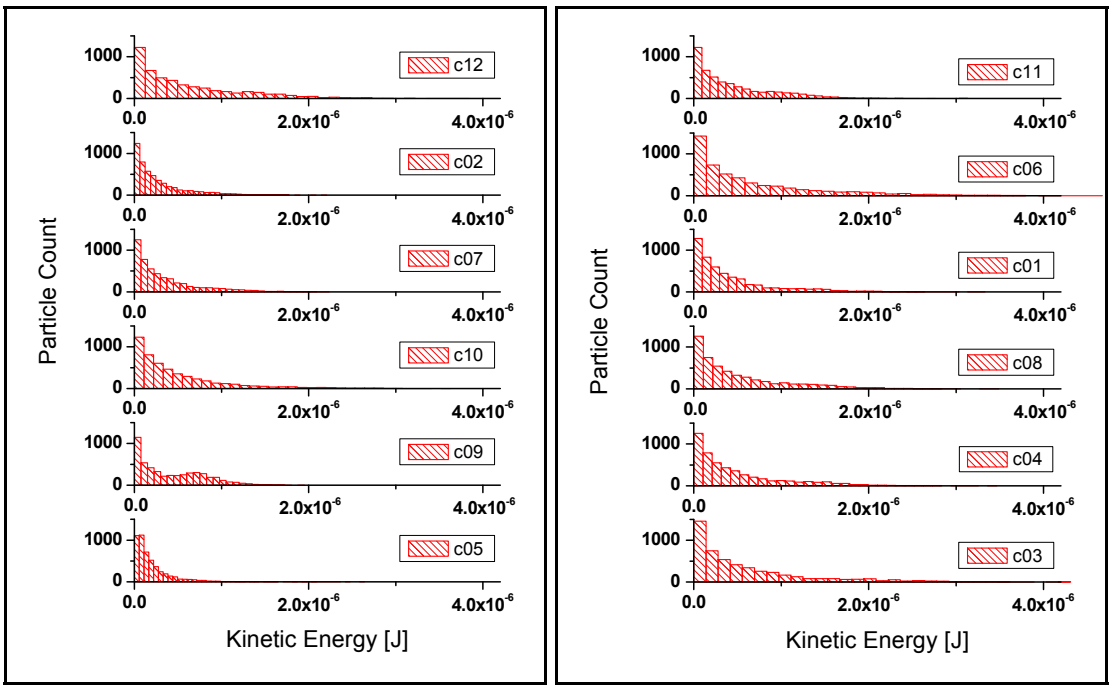

Figure 10.2-8. KE distributions for each condition of YSZ HOSP 2 process map. Scott's formula was used for bin sizing.

Condition	MI Average	MI Standard Deviation	KE Average [J]	KE Standard Deviation [J]
1	0.37	0.58	4.3E-07	4.8E-07
2	0.31	0.31	2.8E-07	3.0E-07
3	0.35	0.60	6.0E-07	6.8E-07
4	0.35	0.51	4.8E-07	5.2E-07
5	0.21	0.22	2.2E-07	2.7E-07
6	0.41	0.77	6.5E-07	7.1E-07
7	0.28	0.28	3.4E-07	3.7E-07
8	0.35	0.55	5.1E-07	5.3E-07
9	0.23	0.18	4.2E-07	3.7E-07
10	0.24	0.38	4.9E-07	5.4E-07
11	0.45	0.71	4.5E-07	4.5E-07
12	0.33	0.51	6.1E-07	6.1E-07

Figure 10.2-9. Average MI and KE values with their standard deviations for YSZ HOSP 2 calculated from DPV 2000 data.

References

1. Padture, N.P., *Thermal Barrier Coatings for Gas-Turbine Engine Applications.* Science, 2002. **296**(12 April): p. 280-284.
2. Bertrand, G., *Low conductivity plasma sprayed thermal barrier coatings using hollow psz spheres: Correlation between thermophysical properties and microstructure.* Surface and Coatings Technology, 2007. **202**.
3. Chi, W., *Microstructure–Thermal Conductivity Relationships for Plasma-Sprayed Yttria-Stabilized Zirconia Coatings.* The American Ceramic Society, 2008. **91**(8): p. 2636-2645.
4. Marple, B.R., *Processing and Properties of Yttria-Stabilized Zirconia TBCs Produced Using Nitrogen as Primary Plasma Gas.* Thermal Spray 2007: Global Coating Solutions, 2007.
5. Chi, W., S. Sampath, and H. Wang, *Microstructure-Thermal Conductivity Relationships for Plasma-Sprayed Yttria Stabilized Zirconia Coatings.* Journal of the American Ceramic Society, 2008. **91**(8): p. 2636-2645.
6. Chi, W., S. Sampath, and H. Wang, *Ambient and High-Temperature Thermal Conductivity of Thermal Sprayed Coatings.* Journal of Thermal Spray Technology, 2006. **15(4)**(December 2006): p. 773-778.
7. Nakamura, T. and Y. Liu, *Determination of nonlinear properties of thermal sprayed ceramic coatings via inverse analysis.* International Journal of Solids and Structures, 2006. **44**(2007): p. 1990-2009.
8. LeMessurier, J. *An aircraft capable of bombing any target on earth within two hours...* 2007 [cited 2009 May 19]; Available from: www.firstscience.com.
9. Johner, G., *Thermal barrier coatings for jet engine improvement.* Thin Solid Films, 1984. **119**(3): p. 301-315.
10. *Zirconia (Zirconium Oxide) and Partially Stabilized Zirconia*. 2008 [cited 2009 January 19]; Available from: http://www.stanfordmaterials.com/zr.html.
11. Sampath, S., *Thermal sprayed ceramic coatings: fundamental issues and application considerations*. 2008, Center for Thermal Spray Research, State University of New York: Stony Brook. p. 23.
12. Claudio, W. *Sulzer Metco - Thermal Spray*. 2009 [cited 2009 May 17]; Available from: http://www.sulzermetco.com/en/DesktopDefault.aspx/tabid-1740//3392_read-5304/.
13. Srinivasan, V., *A Critical Assessment of In-Flight Particle State During Plasma Spraying of YSZ and its Implications on Coating Properties and Process Reliability*, in *Material Science and Engineering*. 2007, SUNY Stony Brook: Stony Brook. p. 201.
14. Fincke, J.R. and R.A. Neiser. *Advanced Diagnostics and Modeling of Spray Processes*. MRS Bulletin 2000 [cited 2000 July 17]; July 2000:[Available from: www.mrs.org/publications/bulletin.
15. Fincke, J.R., *Particle Temperature Measurement in the Thermal Spray Process.* Journal of Thermal Spray Technology, 2001. **Volume 10(2)**(June): p. 255-266.
16. Lucpouliot. *DPV-2000 Reference Manual*. 2005 [cited 2009 March 15]; Available from: http://www.tecnar.com/DATA/DOCUMENT/DPV-manuel_rev5.pdf.

17. Lucpouliot. *DPV Calculation Pronciples*. 2006 [cited 2009 March 15]; Available from: http://www.tecnar.com/DATA/DOCUMENT/DPV_Calculation_Principles.pdf.
18. mhugueny. *Accuraspray-g3 Product Manual*. 2006 [cited 2009 March 15]; Available from: http://www.tecnar.com/DATA/DOCUMENT/MAN%2040857%20EN%2005.pdf.
19. Vaidya, A., Streibl, T., Li, L., Sampath, S., Kovarik, O., Greenlaw, R., *An integrated study of thermal spray process-structure-property correlations: A case study for plasma sprayed molybdenum coatings.* Materials Science and Engineering: A, 2005. **403**(1-2): p. 191-204.
20. Vaidya, A., *Process Maps for Plasma Spraying of Yttria Stabilized Zirconia: An Integrated Approach to Design,Optimization and Reliability*. 2007.
21. Khan, A.N., *Manipulation of air plasma spraying parameters for the production of ceramic coatings.* Journal of Materials Processing Technology, 2008.
22. Scrivani, A., *Enhanced thick thermal barrier coatings that exhibit varying porosity.* Materials Science and Engineering, 2008. **A 476**: p. 1-7.
23. Wan, Y.P., *Numerical Investigation of the Effects of Voltage Fluctuations on the Behavior of Plasma Sprayed Particles*. 2004, State University of New York: Stony Brook.
24. Kucuk, A., Berndt, C.C. , Senturk, U., Lima, R.S., *Influence of plasma spray parameters on mechanical properties of yttria stabilized zirconia coatings. II: Acoustic emission response.* Material Science and Engineering, 2000. **A284**: p. 41-50.
25. Kucuk, A., Berndt, C.C., Senturk, U., Lima, R.S., Lima, C.R.C, *Influence of plasma spray parameters on mechanical properties of yttria stabilized zirconia coatings. I: Four point bend test.* Material Science and Engineering, 2000. **A284**: p. 29-40.
26. Srinivasan, V., *Particle Injection in Direct Current Air Plasma Spray: Salient Observations and Optimization Strategies.* Plasma Chem Plasma Process, 2007. **27**: p. 609-623.
27. Devasenapathi, A., Ang, C. B., Yu, S. C. M., Ng, H. W., *Role of particle injection velocity on coating microstructure of plasma sprayed alumina -- validation of process chart.* Surface and Coatings Technology, 2001. **139**(1): p. 44-54.
28. Zhang, H. *Melting Behavior of In-flight Particles and Its Effects on Splat Morphology in Plasma Spraying*. in *ASME International Mechanical Engineering Congress and Exposition*. 2002. New Orleans, Louisiana.
29. Box, G.E.P., *Statistics for Experimenters. An Introduction to Design, Data Analysis, and Model Building.* 1978, New York: John Wiley & Sons.
30. Streibl, T., Vaidya, A., Friis, M., Srinivasan, V., Sampath, S., *A Critical Assessment of Particle Temperature Distributions Suring Plasma Spraying: Experimental Results for YSZ.* Plasma Chemistry and Plasma Processing, 2005. **26**(1).
31. Scott, D.W., *On optimal and data-based histograms.* Biometrika, 1979. **66**(3): p. 605-610.

32. Sampath, S., Jiang, X., Kulkarni, A., Matejicek, J., Gilmore, D. L., Neiser, R. A., *Development of process maps for plasma spray: case study for molybdenum.* Materials Science and Engineering A, 2003. **348**(1-2): p. 54-66.
33. S. Sampath, V.S., A.Valarezo, A. Vaidya and T. Streibl, *Sensing, Control and Insitu Measurement of Coating Properties: An Integrated Approach towards Establishing Process-Property Correlations.* (In Review).
34. Streibl, T., Vaidya, A., Friis, M., Srinivasan, V., Sampath, S., *A Critical Assessment of Particle Temperature Distributions Suring Plasma Spraying: Experimental Results for YSZ.* Plasma Chemistry and Plasma Processing, 2006. **26**(1).
35. Vardelle, M., *Controlling Particle Injection in Plasma Spraying.* Journal of Thermal Spray Technology, 2001. **Volume 10(2)**(June): p. 267-284.
36. Srinivasan, V. *On the Reproducibility of Air Plasma Spray Process and Control of Particle State*. in *2006 International Thermal Spray Conference*. 2006. Seattle, WA: ASM International.
37. Friis, M. and C. Peerson, *Control of Thermal Spray Processes by Means of Process Maps and Process Windows.* Journal of Thermal Spray Technology, 2001. **12(1)**(March 2003): p. 44-52.